AGU PUBLICATIONS

JGR

Journal of Geophysical Research: Oceans

RESEARCH ARTICLE

10.1002/2014JC010491

River-tide dynamics: Exploration of nonstationary and nonlinear tidal behavior in the Yangtze River estuary

Leicheng Guo[1,2], Mick van der Wegen[2,3], David A. Jay[4], Pascal Matte[5], Zheng Bing Wang[1,3,6], Dano Roelvink[2,3,6], and Qing He[1]

[1]State Key Laboratory of Estuarine and Coastal Research, East China Normal University, Shanghai, China, [2]UNESCO-IHE, Delft, Netherlands, [3]Deltares, Delft, Netherlands, [4]Department of Civil and Environmental Engineering, Portland State University, Portland, Oregon, USA, [5]Centre Eau Terre Environment, Institut National de la Recherche Scientifique, Quebec City, Quebec, Canada, [6]Civil Engineering and Geosciences Faculty, Delft University of Technology, Delft, Netherlands

Key Points:
- Nonstationary river tidal dynamics are quantified using HA and CWT methods
- M_4 amplitude is larger upriver in dry season but larger downriver in wet season
- Amplitude maxima of fortnightly tides occur upriver due to longer wavelength

Correspondence to:
L. Guo,
leicheng120@126.com

Citation:
Guo, L., M. van der Wegen, D. A. Jay, P. Matte, Z. B. Wang, D. Roelvink, and Q. He (2015), River-tide dynamics: Exploration of nonstationary and nonlinear tidal behavior in the Yangtze River estuary, *J. Geophys. Res. Oceans*, *120*, 3499–3521, doi:10.1002/2014JC010491.

Received 8 OCT 2014
Accepted 13 APR 2015
Accepted article online 15 APR 2015
Published online 19 MAY 2015

Abstract River-tide dynamics remain poorly understood, in part because conventional harmonic analysis (HA) does not cope effectively with nonstationary signals. To explore nonstationary behavior of river tides and the modulation effects of river discharge, this work analyzes tidal signals in the Yangtze River estuary using both HA in a nonstationary mode and continuous wavelet transforms (CWT). The Yangtze is an excellent natural laboratory to analyze river tides because of its high and variable flow, its length, and the fact that there are do dams or reflecting barriers within the tidal part of the system. Analysis of tidal frequencies by CWT and analysis of subtidal water level and tidal ranges reveal a broad range of subtidal variations over fortnightly, monthly, semiannual, and annual frequencies driven by subtidal variations in friction and by variable river discharges. We employ HA in a nonstationary mode (NSHA) by segregating data within defined flow ranges into separate analyses. NSHA quantifies the decay of the principal tides and the modulation of M_4 tide with increasing river discharges. M_4 amplitudes decrease far upriver (landward portion of the estuary) and conversely increase close to the ocean as river discharge increases. The fortnightly frequencies reach an amplitude maximum upriver of that for over tide frequencies, due to the longer wavelength of the fortnightly constituents. These methods and findings should be applicable to large tidal rivers globally and have broad implications regarding management of navigation channels and ecosystems in tidal rivers.

1. Introduction

1.1. River Tidal Dynamics

Understanding of tidal wave propagation and tidal properties of estuaries is of broad scientific and societal importance for tidal prediction and management of navigation channels and estuarine ecosystem [*Dronkers*, 1986; *Friedrichs and Aubrey*, 1994; *Kukulka and Jay*, 2003b; *Buschman et al.*, 2009]. Tidal waves propagating from oceans and shelves to coasts and estuaries are modified by shallow water friction, basin topography (estuarine length and convergence in width and depth), and river discharge [e.g., *Jay*, 1991; *Friedrichs and Aubrey*, 1994; *Li and O'Donnell*, 2005; *Lanzoni and Seminara*, 1998; *Godin*, 1999; *van Rijn*, 2011]. Depending on the balance between friction, channel convergence, and river flow, the amplitudes of the principal tidal constituents may reduce, increase, or remain constant during the landward propagation [e.g., *Jay*, 1991; *Friedrichs and Aubrey*, 1994; *Savenije et al.*, 2008]. The same factors will cause nonlinearly generated low (subtidal) and high (overtide) frequencies to behave differently from astronomical constituents [*Gallo and Vinzon*, 2005; *Matte et al.*, 2014]. We argue here that the differences in wavelength of various tidal species are also important in long estuaries.

Tidal waves impinging from the ocean are distorted as they move into coastal and estuarine waters. Since wave celerity is a function of water depth in shallow waters, faster high water propagation and slower low water propagation lead to tidal wave deformation that is reflected in unequal durations of rising and falling water levels and peak ebb and flood currents [*Speer and Aubrey*, 1985; *Friedrichs and Aubrey*, 1988]. In harmonic terms, tidal distortion is expressed by the interaction between astronomical constituents and their overtides. Distortion of the semidiurnal M_2 tide, for example, gives rise to overtides such as M_4, M_6, and M_8 at 2×, 3×, and 4× of the frequency of M_2 [*Pugh*, 1987; *Parker*, 1991; *Le Provost*, 1991; *Walters and Werner*, 1991;

Wang et al., 1999]. Interaction between M_2 and M_4 leads to widely observed tidal distortion and asymmetry on a 12.42 h time scale because M_2 is the largest astronomical constituent in most regions and M_4 is the dominant overtide [*Pugh*, 1987; *Friedrichs and Aubrey*, 1988]. Interactions between different astronomical constituents generate a series of compound overtides [*Parker*, 1991; *Wang et al*., 1999], and these may also contribute tidal asymmetry [*Song et al*., 2011]. For instance, the semidiurnal constituents M_2 and S_2 interact to generate a quarter-diurnal MS_4 tide (T = 6.1033 h) and a fortnightly MSf (T = 14.7653 days) tide [*Aubrey and Speer*, 1985; *Parker*, 1991]. The fortnightly MSf tide is often substantial (amplitude > 0.1 m) in tidal rivers [*Aubrey and Speer*, 1985] but its behavior has been little examined because of its long wavelength and difficulties in separating the fortnightly signals from effects of variable river flow. Significant fortnightly subtidal water level variations are typically found in tidal rivers, causing lower mean water levels (MWL) on neap tides than on spring tides [*Speer and Aubrey*, 1985; *Buschman et al*., 2009; *Sassi and Hoitink*, 2013; *Jay et al*., 2014]. Though it is known that both overtides and compound tides affect tidal asymmetry in varying time scales; however, their behavior in response to varying river discharges in tidal rivers has been given less attention.

River discharge strongly alters tidal propagation by reducing tidal amplitude, delaying wave propagation, and altering energy distribution between tidal frequencies [*Godin*, 1985, 1991, 1999; *Jay and Flinchem*, 1997; *Horrevoets et al.,* 2004]. *Jay* [1991] and *Jay and Flinchem* [1997] suggested that river tides (river-modulated tides in estuaries) have complex behavior in several aspects: (1) strong frictional damping by a river flow; (2) variable interaction of barotropic tide with itself through nonlinearities in bed stresses that are modulated by a river flow; (3) topographic funneling of tidal waves in a predominantly convergent fluvial geometry; (4) incident and reflected waves of each species; and (5) bodily advection of the tide by a river flow. A higher river discharge progressively attenuates tidal energy and reduces tidal range via enhanced tidal friction [*LeBlond*, 1978; *Godin*, 1985, 1991, 1999; *Savenije et al*., 2008; *Savenije*, 2005; *Cai et al*., 2012]. Tidal damping is frequency-dependent such that higher frequencies are damped faster spatially by a river flow even as they are being generated [*Godin*, 1985, 1991], reaching a point upstream where they are damped even faster than they are being generated [*Matte et al*., 2014].

River discharge is rarely constant. It can vary rapidly, sometimes over a large range. A time-varying river discharge induces strong nonstationary behavior in tidal signals [*Flinchem and Jay*, 2000; *Jay and Kukulka*, 2003]. Capturing the nonstationary features of river tides and incorporating them into an analytical model to distinguish tidal (banded) from nontidal (broadband) variations is difficult [*Matte et al*., 2013]. Thus, it remains a challenge to examine nonstationary river tidal characteristics.

1.2. Tidal Analysis for Nonstationary Systems

Tidal dynamics have been extensively studied through tidal analysis and multiple modeling techniques. Traditional methods for analyzing tidal signals include harmonic analysis (HA) and Fourier analysis. The HA method, introduced in the late nineteenth century [e.g., *Darwin*, 1891], was improved as knowledge of tidal potential developed [*Doodson*, 1921] through application of inverse techniques and robust confidence estimation methods, and by the introduction of improved inference and nodal modulation procedures [*Foreman*, 1977; *Foreman et al*., 2009; *Pawlowicz et al*., 2002; *Leffler and Jay*, 2009; *Matte et al*., 2013]. The HA method makes primary assumptions: (1) tides are stationary and independent of other oceanic and atmospheric influences; (2) there is a fixed number of tidal constituents with discrete periodicities, phase angles, and amplitudes; and (3) tidal constituents are mutually independent [*Dean*, 1966; *Godin*, 1972; *Jay and Flinchem*, 1997; *Flinchem and Jay*, 2000]. HA determines the amplitudes and phases of a number of tidal constituents with predetermined frequencies defined by tidal potential [*Doodson*, 1921] via a least-square-fit applied to the measured tidal heights. An important limitation of the HA method is the data length required to resolve subfrequency tides (frequency lower than diurnal tides) and to distinguish tidal constituents within close frequency intervals, the so-called Rayleigh criterion [*Godin*, 1972].

The stationary assumption of the HA method is approximately valid for oceanic tides in deep waters. However, coastal tides are chaotic [*Frison et al*., 1999] and often subjected to nonstationary interactions with meteorological forcing and river discharge [*Jay and Flinchem*, 1997]. Tidal harmonic constants may vary over the analysis period in tidal rivers; thus, conventional HA will leak energy from major constituents to their neighboring frequencies [*Foreman et al*., 1995]. Amplitude and phase variability during an HA window also reduces the estimated amplitudes [*Zaron and Jay*, 2014]. In practice, it is still possible to perform a short-term HA (e.g., HA on a data length of 30 days) to resolve major tidal constituents provided that the

nontidal forcing varies little during the data window period. When river discharge variability is high, however, HA will provide inaccurate results because of the nonlinearly and mutually dependent behaviors of nearby tidal spectral bands [*Godin*, 1999; *Jay and Flinchem*, 1997, 1999]. Also, because tidal currents are more sensitive than water levels to nonstationary variations, HA of current records has been less successful than for water level records [*Godin*, 1983]. Overall, short-term HA cannot resolve enough tidal constituents for predictive purposes, and HA on long records hides the nonstationary behavior on time scales of days to seasons and provides no information on variations over time.

Progress in analyzing nonstationary tides has been made in the recent decades. *Jay and Flinchem* [1997] reviewed tidal analysis methods that were applied to nonstationary tides, e.g., species concordance method [*Simon*, 1991] and complex demodulation method (essentially a single-frequency wavelet approach), and found that the continuous wavelet transforms (CWT) is an effective tool in analyzing nonstationary tides. The CWT method (see section 2.3 and Appendix A for details) optimizes time-frequency resolution so that near-instantaneous response of tidal waves to varying river discharges is exposed. Hence, the CWT method is more accurate and efficient than HA in coping with nontidal variations and strong time-varying properties. Application of CWT to the tides of the Columbia River estuary was reported by *Jay and Flinchem* [1997], *Flinchem and Jay* [2000], *Kukulka and Jay* [2003a, 2003b], followed by *Buschman et al*. [2009], *Sassi and Hoitink* [2013], and *Shetye and Vijith* [2013] for other tidal rivers. The basic principles of CWT in analyzing tidal signals were provided in *Jay and Flinchem* [1997, 1999]. A major limitation of the CWT method lies in that it only outputs information regarding tidal species rather than individual tidal constituents. Thus, neither HA or CWT can by itself fully resolve nonstationary tides—HA has limited time resolution and CWT method cannot at present resolve tidal constituents.

1.3. Aim and Methodology

The foregoing review suggests that nonstationary river tides exhibit complex behavior over time and space. But it remains uncertain, for instance, how different tidal constituents or species are modulated in the time, space, and frequency dimensions by unsteady river discharges. Thus in this study, we explore river tidal dynamics regarding damping of astronomical constituents, modulation of shallow water constituents, and the spatial and temporal evolutions of tidal frequency spectra under the influence of nonstationary river discharges. We also explain the mechanisms of tidal-fluvial interaction in terms of tidal and subtidal friction. For this purpose, we analyze long-time series of tidal data in the Yangtze River estuary (YRE) employing both HA and CWT methods. The YRE is a large river system influenced by both highly varying, large river discharge and strong tides with a mixed regime. It provides a natural laboratory for our study, because it is long relative to the tidal wavelength, so that the full resolution of tides upriver can be analyzed, and there is no reflecting dam or other engineered barriers below the head of the tide, so that tidal waves travel landward for hundreds of kilometers and exhibit a broad range of nonstationary behavior that has not previously been documented. The tidal processes analyzed here are, moreover, likely typical of other large tidal systems.

2. Setting, Data, and Methods

2.1. Introduction to the Yangtze River Estuary

The YRE covers the area where the Yangtze River (also called the Changjiang River) meets the East China Sea (Figure 1). Shaped by large river discharges, strong tides, and moderate wind and waves, the YRE now has two major channels connecting to the sea [*Yun*, 2004]. The South Branch is the main channel discharging river flow and accommodating tidal prism, whereas the North Branch delivers limited fresh river water and is a tide-dominated environment; thus, it is excluded in this study.

Traditionally, the YRE has been divided into three reaches, based on the spatial variations of fluvial and tidal energy: (1) an upper estuary between Datong (tidal wave limit) and Jiangyin (405 km downstream Datong) where river forcing dominates; (2) a middle estuary between Jiangyin and Zhongjun (615 km downstream Datong) where both river and tidal processes are important, and (3) a lower estuary seaward of Zhongjun where tidal forcing dominates [*Shen*, 2003, Figure 1]. Datong and Jiangyin are the upstream limits of tidal wave influence and tidal current reversal, respectively, under moderate river and tidal conditions. Some minor tidal oscillations are still observed at Datong during low discharge periods. The river reaches between Jiangyin and Zhongjun are characterized by a seaward increase in channel width from 3 km to nearly

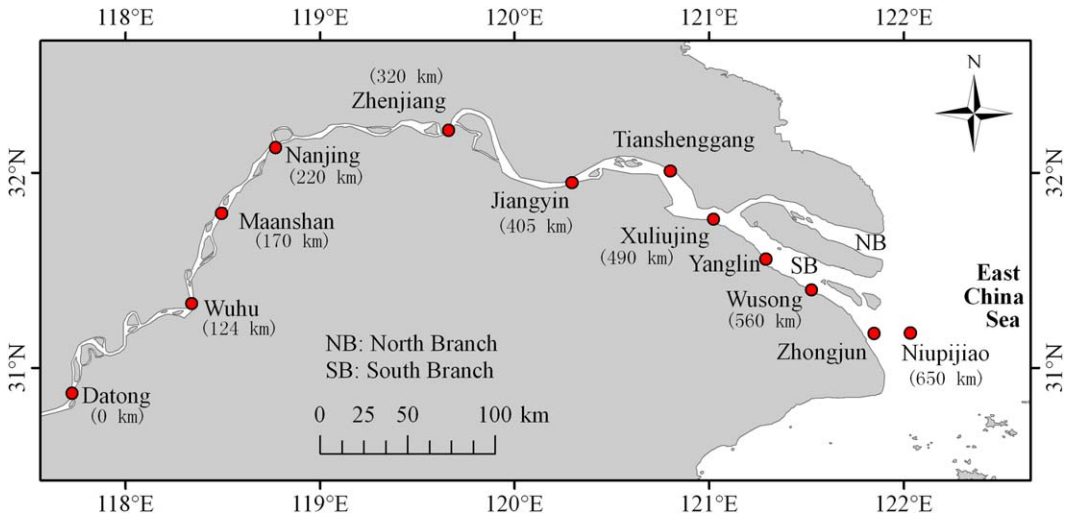

Figure 1. The Yangtze River estuary (YRE) and the location of the tidal gauge stations. The numbers in brackets are distance downward Datong.

20 km, while the reaches between Datong and Jiangyin are nearly uniform in width despite the presence of meanders.

Rive discharge measured at Datong (Figure 1) is huge and variable, primarily on season time scales. From measurements over the past 60 years, the daily river discharge at Datong varies between 6000 and 92,000 m^3/s with an annual mean value of 28,600 m^3/s [*Zhang et al*., 2003]. River stage varies between ~4 and ~16 m for river discharges between ~10,000 and ~80,000 m^3/s at Datong based on data between 1998 and 2013. Thus, a high river discharge greatly increases river stage upstream and produces a longitudinal water level gradient that is 4 times greater than that during low river discharge periods. Interannually, the Yangtze River is subject to alternating high (e.g., flood in 1998) and low (e.g., drought in 2006) flow conditions. Seasonally, the river discharge hydrograph is characterized by a wet season between May and October and a dry season between November and April (see Figure 3a). The durations of high and low river discharges can be several months (instead of in days to weeks as in mountainous rivers), making it easier to distinguish tidal dynamics between high and low river flow conditions.

The Three Gorges Dam (located about 1100 km upstream Datong) has operated since 2003. It has reduced the annual flood peak discharge by up to 20,000 m^3/s while the dry season discharge has increased by 500–2000 m^3/s, considerably flattening the river discharge hydrographs [*Gao et al*., 2013]. Overall, the operation of the Three Gorges Dam does not induce rapid fluctuations of river discharges and water levels at Datong. Also, there is no big tributary in the lower basin downstream Datong though along-channel water withdrawal reduces river discharge to some degree (less than 10%) [*Zhang et al*., 2012], an effect not considered in this study.

Tides from the East China Sea that enter the YRE are mixed, with significant semidiurnal and diurnal components, with an A_{D1}/A_{D2} ratio of ~0.24 (A is amplitude, D_1 refers to the diurnal wave, and D_2 refers to the semidiurnal wave, see below). A mean tidal range of 2.66 m and a spring tidal range up to 5 m are observed at the mouth [*Yun*, 2004]. In the landward direction, tidal waves first amplify and then damp further upstream to the head of the tide at Datong due to the friction and river discharge. The mean tidal prism is 10 times larger than the mean river flow, suggesting that both river discharge and tides are significant forces in the YRE.

Tidal waves are significantly distorted during propagation in the YRE, and this distortion increases landward, resulting in longer falling tides and shorter rising tides (Figure 2). The duration of the falling tide increases from 6.2 h at Niupijiao to 8.6 h at Nanjing on a spring tide in the dry season. A high river discharge reduces tidal ranges and increases tidal deformation relative to a low river discharge. Interestingly, the maximum spring tidal range in the wet season (Figure 2c) may be larger than that in the dry season (Figure 2a) downriver (e.g., at Xuliujing, Yanglin, and Niupijiao), whereas tidal ranges are overall larger in the dry season than

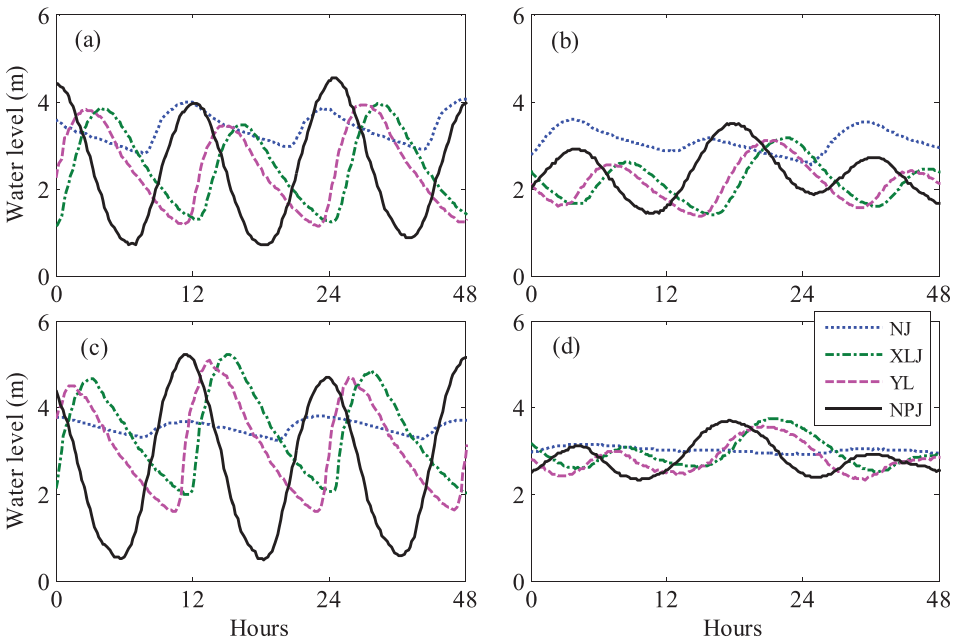

Figure 2. Water levels during: (a) a dry season (~11,000 m^3/s) spring tide; (b) a dry season-neap tide; (c) a wet season (~43,000 m^3/s) spring tide, and (d) a wet season-neap tide at Nanjing (NJ), Xuliujing (XLJ), Yanglin (YL), and Niupijiao (NPJ), based on 2009 data. Water levels are reduced by 4 m in the wet season at Nanjing to facilitate presentation of the data. Niupijiao is representative of coastal tidal conditions.

in the wet season at Nanjing on both spring and neap tides. These variable tidal properties can only be explained via more detailed analysis (see section 3.1).

2.2. Data

Long time series of river discharges and water levels in the YRE were collected from the Bureau of Hydrology, Changjiang Water Resources Commission (CWRC) for detailed analysis in this study. Daily river discharges at Datong was measured between 1998 and 2013. Hourly tidal water levels were provided for an 8 year period between 2006 and 2013 at Nanjing, Xuliujing, Yanglin, and Niupijiao. Irregularly spaced water levels were collected at Zhenjiang and Jiangyin. Although the time resolution of the water levels at Zhenjiang and Jiangyin is too low for in-depth analysis, they still show spring-neap tidal variations (Figure 3). For all stations, the water levels are converted to elevation relative to the Wusong Datum (mean sea level at the coast) from their local reference levels.

Cross-sectionally integrated tidal discharges were measured at Xuliujing by a horizontally mounted ADCP with hourly resolution between September 2009 and August 2010 by the Changjiangkou Hydrological Survey Bureau [*Zhu et al*., 2008] and analyzed by the method of *Hoitink et al*. [2009] and *Buschman et al*. [2009]. The tidal discharge data are converted into cross-sectionally averaged velocities by dividing cross-sectional areas appropriate to the instantaneous water levels. These velocities are used to assess the relative contribution of river discharge and tides to subtidal friction according to the decomposition method proposed by *Buschman et al*. [2009].

2.3. Tidal Analysis Methods

Five types of tidal analysis were conducted, preliminary tidal height analysis (e.g., analysis of subtidal water levels and tidal ranges), HA, NSHA, CWT, and subtidal decomposition of current velocities. First, we estimate two kinds of subtidal water levels, tidal daily and fortnightly MWL by averaging water levels over 25 h and 15 days moving windows, respectively. The 25 h moving average filter captures the low-frequency energy well although it eliminates M_2 signal and passes portions of K_1 and S_2 and other constituents to a minor degree [*Godin*, 1972]. Tidal ranges are estimated in a manner similar to *Kukulka and Jay* [2003a] and *Matte et al*. [2013], by high-pass filtering the hourly water levels to remove variations at subtidal frequencies, interpolating the data to 6 min intervals, and determining the minimum and maximum heights using a 27 h

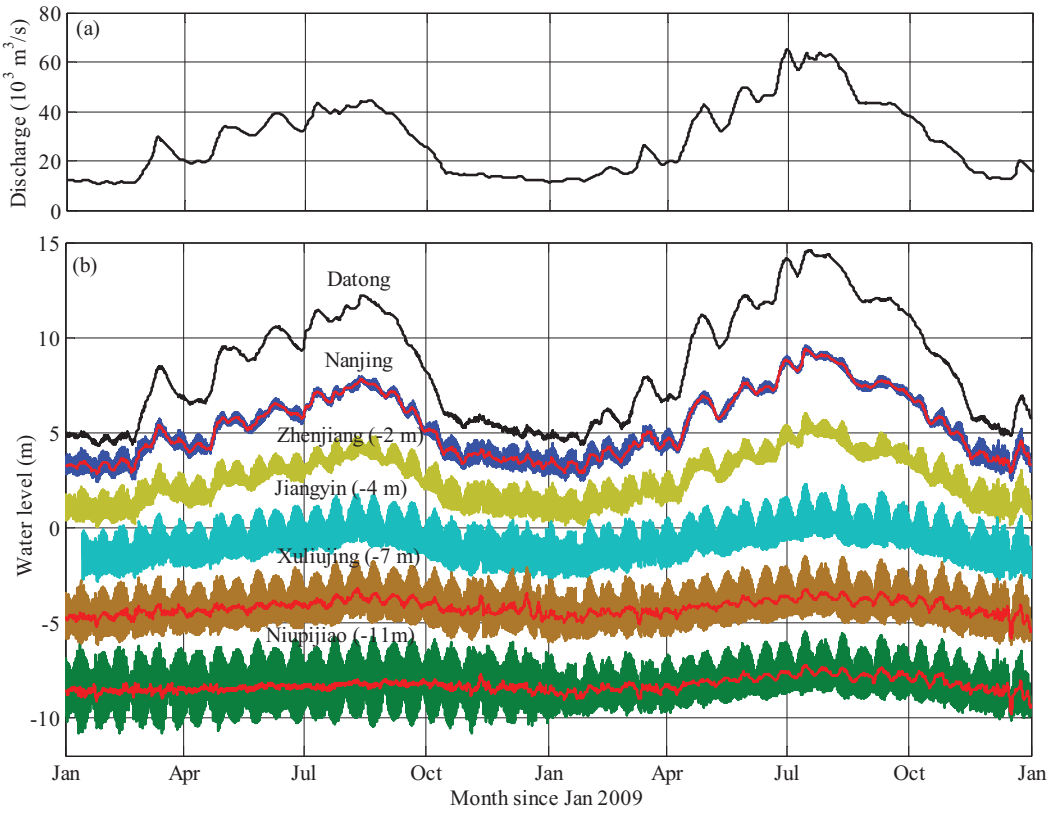

Figure 3. (a) River discharges at Datong and (b) water levels at Datong, Nanjing, Zhenjiang (decreased by 2 m), Jiangyin (deceased by 4 m), Xuliujing, (decreased by 7 m), Niupijiao (decreased by 11 m) between 2009 and 2010. The red lines indicate the daily (24 h) averaged water levels (MWL).

moving window with a 1 h step. The tidal ranges are estimated by the differences between the minimum and maximum water levels in each 27 h window. Results of these preliminary analyses are presented in section 3.1.

Second, we use HA in a long and short-term mode and in a nonstationary mode to estimate amplitudes and phases of tidal constituents based on the T_TIDE function (see Appendix A and *Pawlowicz et al.* [2002]). Long-term HA provides a preliminary impression of the time-averaged tidal properties of individual constituents, but does not resolve the time-varying behavior. The short-term HA (STHA) uses successive, short windows (e.g., 30 days) to provide a time series of tidal outputs for a limited number of constituents. The STHA is limited in the number of constituents and the scales of variability that can be resolved. To overcome this problem, we employ HA in a nonstationary mode (NSHA). NSHA is conducted on tidal levels during the periods when river discharge is within certain ranges. Specifically, NSHA is performed on tidal levels at Nanjing and Xuliujing during the periods when river discharge at Datong is, for example, between 10,000 and 15,000 m^3/s. There is a total of 17,442 h of observations in this range during the 8 year period analyzed, though the periods with this range of flow are discontinuous. Because larger amount of data are used, this approach resolves the major tidal constituents with precision higher than the results from STHA applied to a 30 days record. Similar analyses are conducted for river discharges up to 45,000 m^3/s in an increment of 5000 m^3/s. There are fewer data points for river discharge higher than 45,000 m^3/s; thus, these flow levels are not analyzed (see section 3.3). Note that even with NSHA, some averaging over river discharge occurred, and some behavior related to nonstationarity is not resolved, e.g., any possible lags between discharge and tidal properties.

Third, a CWT method is used to analyze spatial and temporal evolutions of tidal frequency spectra and properties of tidal species. The CWT method applies a wavelet transform as a band-pass filter to a tidal time series of signals. In essence, the CWT is a time variable analog to the Fourier transform, but with lower

frequency resolution. Thus, the one-dimensional input is transformed into a two-dimensional output in time and frequency, resolving both the dominant frequency modes and the variations of these modes over time [*Jay and Flinchem*, 1997; *Torrence and Compo*, 1998]. CWT analysis is able to resolve different tidal species, e.g., the diurnal (D_1), semidiurnal (D_2), and quarter-diurnal (D_4) bands, but not tidal constituents (e.g., M_2 and O_1 tides) within species. The CWT method is also applied to the time series of tidal currents, allowing decomposition of those currents into a residual (subtidal) component and several tidal species. Details of the CWT method and the settings are described in the Appendix A, and results of CWT are presented in section 3.2.

Finally, to explain the development of subtidal variations in MWL, we use the current velocities to estimate subtidal friction components caused by river flow, river-tide interaction, and tidal asymmetry according to the subtidal momentum decomposition method in *Buschman et al*. [2009] (see Appendix A). This analysis will expose the relationship between subtidal variations of tidal currents, friction, and water level fluctuations (see section 3.4).

3. Results

3.1. Subtidal Variations

Fluctuating river flow causes large seasonal variations of MWL along the YRE. Figure 3 shows a 2-year time series of river discharges and water levels at Datong along with tidal water levels at five stations downstream Datong. River discharge varies in a seasonal pattern typical of most years. Water levels are elevated significantly in the wet season (Figure 3b). Seasonal MWL variations decrease in the downstream direction, but are still evident at Niupijiao, where the MWL is ~0.4 m higher in the wet season (~43,000 m^3/s) than in the dry season (~11,000 m^3/s).

Daily MWL is systematically lower on neap tides than on spring tides in the reaches between Nanjing and Xuliujing, although this phenomenon is less evident at Niupijiao (Figure 3b). This phenomenon indicates that fortnightly subtidal water level variations in the upstream region of the estuary are strong. Additionally, although the highest high waters in a spring-neap tidal cycle typically occur on spring tides at all stations from Nanjing to Niupijiao, the opposite is not true for the lowest low waters. Specifically, the lowest low waters occur on neap tides at more landward stations (e.g., at Nanjing and Zhenjiang), whereas the lowest low waters still occur on spring tides at more seaward stations (e.g., at Xuliujing and Niupijiao) as they typically do in coastal, tide-dominated environments [*LeBlond*, 1979; *Gallo and Vinzon*, 2005]. The source of this phenomenon is that the fortnightly changes in daily MWL grow upriver and become larger than tidal monthly variations in tidal range. Lower low waters on neap tides are observed at Zhenjiang but not at Jiangyin, suggesting that the fortnightly variations of the daily MWL become prominent upstream Zhenjiang, while the fortnightly variations of tidal ranges (in spring-neap cycles) dominate at more seaward stations.

Tidal ranges exhibit strong temporal variations, e.g., fortnightly variations corresponding to the spring-neap tidal cycles (Figure 4a). Spring tidal ranges are about ~2.21 and ~1.36 m larger than neap tidal ranges at Niupijiao and Xuliujing, respectively. Moreover, the spring-neap variations in tidal ranges are rather irregular, so that the tidal ranges of successive spring or neap tides are unequal, indicating tidal monthly variations. On average, spring tidal ranges are ~0.48 and ~0.34 m larger than the preceding or succeeding spring tidal ranges at Niupijiao and Xuliujing, respectively. Similar variations occur for neap tides. Seasonally, tidal ranges decrease remarkably in the wet season at Nanjing, following the river discharge hydrograph, whereas the influence of rive flow is less obvious at Niupijiao. Moreover, spring tidal ranges typically reach seasonal maxima in February–March and August–September when the tidal range differences between spring and neap tides at the ocean entrance are also maximal (i.e., at Niupijiao). These monthly and seasonal variations in tidal ranges explain why spring tidal ranges in the wet season (e.g., in August) are larger than in the dry season (e.g., in January) as observed in Figure 2. Figure 4a also shows that neap tidal ranges at Niupijiao and Xuliujing are nearly the same (especially between February and April and between August and October), whereas spring tidal ranges are overall much larger at Niupijiao than Xuliujing. This suggests that spring tides are much more attenuated in the landward direction than neap tides. In other words, there are strong fortnightly and seasonal variations in tidal damping rate in the landward direction. This phenomenon is also reflected by a landward decrease of A_{S2}/A_{M2} amplitude ratio from Niupijiao (~0.45) to Nanjing (~0.40) (Table 1). *Jay et al*. [1990] noted a similar upriver decreasing of A_{S2}/A_{M2} in the Columbia River. *Godin*

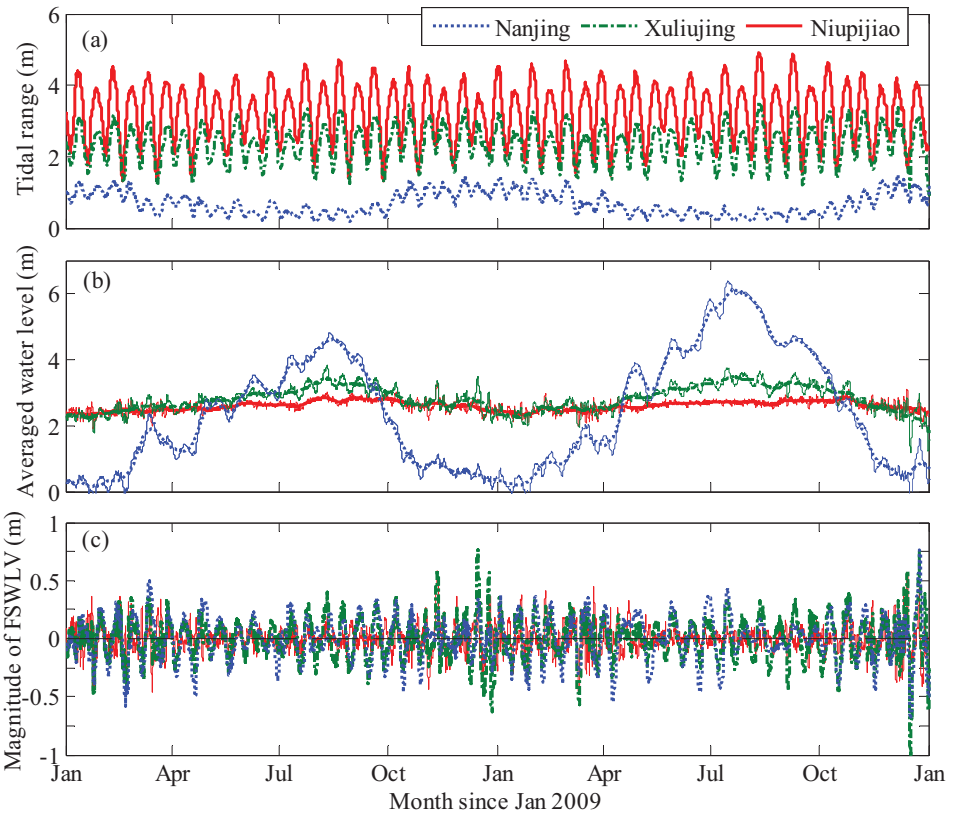

Figure 4. For Nanjing, Xuliujing, and Niupijiao, temporal variations of (a) tidal ranges, (b) daily averaged (thin lines), and fortnightly averaged (thick lines) subtidal water levels, and (c) magnitude of the fortnightly subtidal water level variations in 2009. The daily and fortnightly averaged water levels at Nanjing are reduced by 3 m. FSWLV indicates fortnightly subtidal water level variations.

[1999] indicated that most linear tidal constituents damp more rapidly than M_2 in a tidal river, though some may also be increased by nonlinear energy transfer or resonance. This occurs because the along-channel tidal energy flux is quadratic with tidal range while dissipation is cubic so that tides decay more rapidly on spring tides than on averaged or neap tides [*Jay et al*., 1990].

Figure 4b shows temporal variations of fortnightly and daily MWL. The fortnightly MWL demonstrates seasonal variations following seasonal river discharge fluctuations. The daily MWL exhibits significant fortnightly variations. The differences between the daily MWL and fortnightly MWL represent the magnitude of the fortnightly subtidal water level variations, which can be as large as ~1.0 m (Figure 4c). Linking Figures 4a and 4c, positive and negative variations in fortnightly subtidal water levels correspond to the spring and neap tides, respectively, indicating that the daily MWL on spring tides can be ~1.0 m higher than on neap tides. The amplitudes of fortnightly variations are generally smaller in the wet season because a high river discharge damps the tides substantially. Spatially, the maximum amplitude of the fortnightly fluctuations usually occurs between Zhenjiang and Nanjing. At Niupijiao, there are less regularity and more spikiness in the fortnightly subtidal water level variations, which may be attributed to atmospheric influences. In summary, tidal signals in the YRE exhibit strong tidal fortnightly, monthly, and seasonal variations in subtidal water levels and tidal ranges. Fluctuations in MWL are primarily due to tidal-fluvial processes landward of Niupijiao, but coastal processes become more prominent close to the ocean. This along-channel gradient in the dominant forcing processes is typical of river estuaries [*Jay et al*., 2014].

3.2. Time-Frequency Analysis of Tidal Species

CWT analysis displays temporal and spatial evolutions of tidal frequency spectra. The incoming oceanic tides at Niupijiao contain primarily D_2 and D_1 energy (Figure 5a). A D_4 tide is generated inside the estuary and becomes important at Xuliujing (Figure 5b). The D_4 tide covaries with the D_2 tide over the spring-neap tidal cycles. At the same time, significant fortnightly tidal signals as well as monthly signals are also

Table 1. Long-Term Average Tidal Properties: Tidal Amplitudes (A) and Phases (P) of Major Diurnal, Semidiurnal, and Quarter-Diurnal Tides and Subtidal Frequencies at Niupijiao, Yanglin, Xuliujing, and Nanjing Determined by HA of 8 Year Records

		Niupijiao		Yanglin		Xuliujing		Nanjing	
		A (m)	P (°)	A (m)	P (°)	A (m)	P (°)	A (m)	P (°)
Sub	Sa	0.173	227	0.310	209	0.417	209	1.889	199
	Ssa	0.040	46	0.044	331	0.049	310	0.324	265
	MSm	0.024	123	0.010	160	0.014	194	0.044	210
	Mm	0.012	201	0.036	25	0.044	26	0.078	38
	MSf	0.026	200	0.115	52	0.140	56	0.205	72
	Mf	0.003	338	0.026	12	0.036	16	0.039	78
D1	O_1	0.16	140	0.14	175	0.14	191	0.06	318
	K_1	0.28	185	0.22	229	0.21	248	0.07	20
	P_1	0.09	192	0.07	236	0.06	248	0.02	28
D2	M_2	1.30	305	0.93	42	0.90	78	0.22	305
	S_2	0.59	350	0.40	89	0.38	127	0.09	357
	N_2	0.23	289	0.16	25	0.15	61	0.04	281
D4	M_4	0.037	180	0.196	0	0.168	77	0.061	162
	MS_4	0.019	241	0.163	50	0.139	127	0.050	216
	MN_4	0.017	155	0.067	341	0.057	58	0.021	137

detected at Xuliujing. Farther upstream, the D_1 and D_2 tidal energy are attenuated to a large extent at Nanjing (Figure 5c). Tidal decay is much stronger during the high river discharge period (between June and September). Simultaneously, the fortnightly signals gain strength. At Datong, the tidal signal is very small and little fortnightly tidal signal remains; only the seasonal signals are still significant, forced by fluctuating river discharges (Figure 5d). Overall, the CWT results illustrate landward decay of oceanic (i.e., D_1 and D_2) tides and internal generation of both supra and subfrequencies. The strong fortnightly frequency signals do not originate from river flow or oceanic tides but are mainly generated inside the estuary because there is very little energy at the fortnightly frequencies in the oceanic tides and in the river flow. Similarly tidal monthly signals can be also internally generated but they are poorly separated from the monthly fluctuations in oceanic tides and river flow.

Figure 6 shows time-averaged (over the year of 2009) wavelet power structure determined by CWT at Niupijiao, Xuliujing, and Nanjing. It is evident that tidal daily variance (the summed wavelet power of the D_1 and D_2 bands) dominates at Niupijiao, with another peak in the annual band but no significant energy in the quarterdiurnal and fortnightly bands. The tidal daily variations decrease in the upstream direction, whereas the low-frequency and overtide (e.g., D_4) bands gain wavelet power upriver, especially the fortnightly and annual bands. The tidal daily variance explains 97.2% of the total variance (integrated wavelet power over the complete frequency spectrum) at Niupijiao, but only 76.8 and 1.6% at Xuliujing and Nanjing, respectively. Thus, there is a landward decrease of tidal daily oscillations and a landward increase of low-frequency and overtide oscillations. Note that the D_4 amplitude is maximal in the lower part of the estuary, around Yanglin.

We further quantify the D_1, D_2, and D_4 amplitudes by summing the weighted wavelet power and converting to wavelet amplitude based on equation (A5). Figure 7 shows strong fortnightly and monthly variations in the amplitudes of three tidal species. Landward decay of the D_1 and D_2 tides is evident upstream Niupijiao, whereas the D_4 amplitude increases remarkably from Niupijiao to Xuliujing before it decreases upstream Xuliujing. The seasonal amplitude decreases of the D_1, D_2, and D_4 tides caused by a high river discharge in the wet season are particularly evident at Nanjing, and D_4 amplitude covaries with the D_2 tide but not the D_1 tide. The D_1, D_2, and D_4 amplitudes covary only during the period when the amplitudes of subtidal water level (e.g., D_f and D_m) variations are small (approximately between May and July between November and December). The tidal monthly signals in Figure 6 are, however, contaminated by river flow fluctuations at Datong and by coastal processes at Niupijiao; thus, they do not represent purely tidal effects.

Semiannual variations in tidal strength are also evident, though they are not as strong as the fortnightly variations. Figure 4a shows that the spring tidal ranges tend to be larger and neap tidal ranges tend to be smaller between February and March and between August and September, than during the other months. Figure 7 again shows larger spring-neap tidal amplitude variations around March and September. These

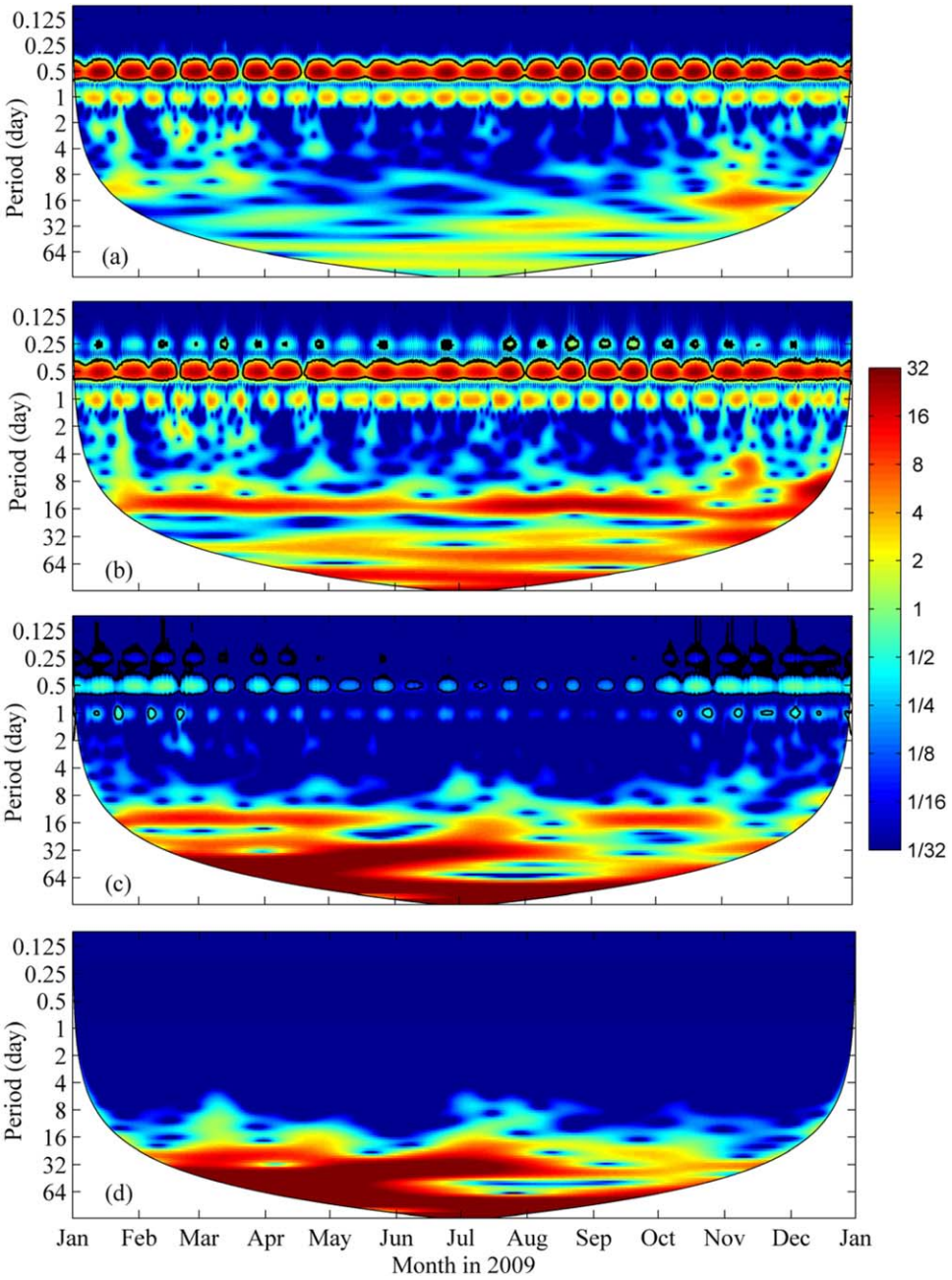

Figure 5. Continuous wavelet power spectra of time series of water levels at (a) Niupijiao, (b) Xuliujing, (c) Nanjing, and (d) Datong in 2009. The wavelet power is $log_2(A^2/v)$, where A is the wavelet amplitude, v is the variance of the original tidal signals. The y axis is on a $log2$ scale. The cone of influence is indicated by the white area by 95% confidence level due to the edging effects. The thick black contour encloses regions of greater than 95% confidence for a red noise process with a lag-1 coefficient of 0.72.

semiannual variations are most obvious at Niupijiao and Xuliujing where tidal oscillations dominate. Comparison between Figures 7a–7c indicates that the semiannual variation pattern is out of phase with river discharge fluctuations. Instead, the semiannual variations stem primarily from oceanic tides (reflected by tidal signals at Niupijiao). This phenomenon may be a surface manifestation of the internal tides in the East China Sea [*Lien et al.*, 2013], but merits future study because seasonal variations of these internal tides are not well documented. Alternatively, it could be associated with seasonal changes in winds, wind waves, and coastal water levels.

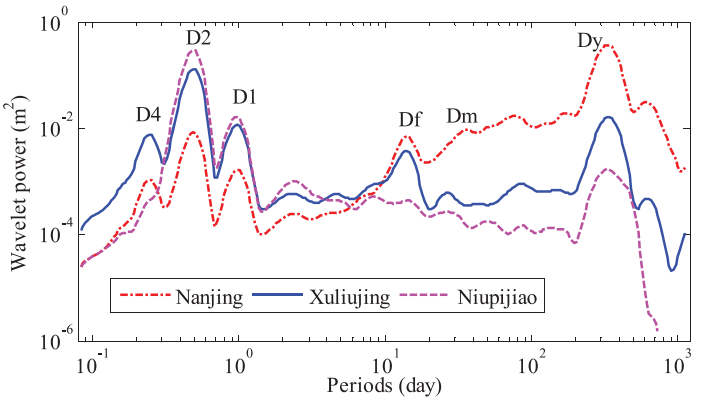

Figure 6. CWT-determined wavelet power spectrum (scaled by the frequencies and presented in log-log axis) by averaging over time at Nanjing, Xuliujing, and Niupijiao. Df, Dm, and Dy indicate frequencies in the fortnightly, monthly, and yearly bands.

3.3. Frequency Structure of Tidal Constituents

We apply HA to resolve tidal constituents from the tidal species. Long-term HA on 8 year data (resolving 69 constituents) indicates that tidal oscillations explain 98, 93, and 76% of the water level variations at Niupijiao, Xuliujing, and Nanjing, captured by HA, respectively. These ratios differ somewhat from the CWT power estimates in section 3.2, because the CWT power estimates include all frequencies, whereas the HA estimates only capture narrow-

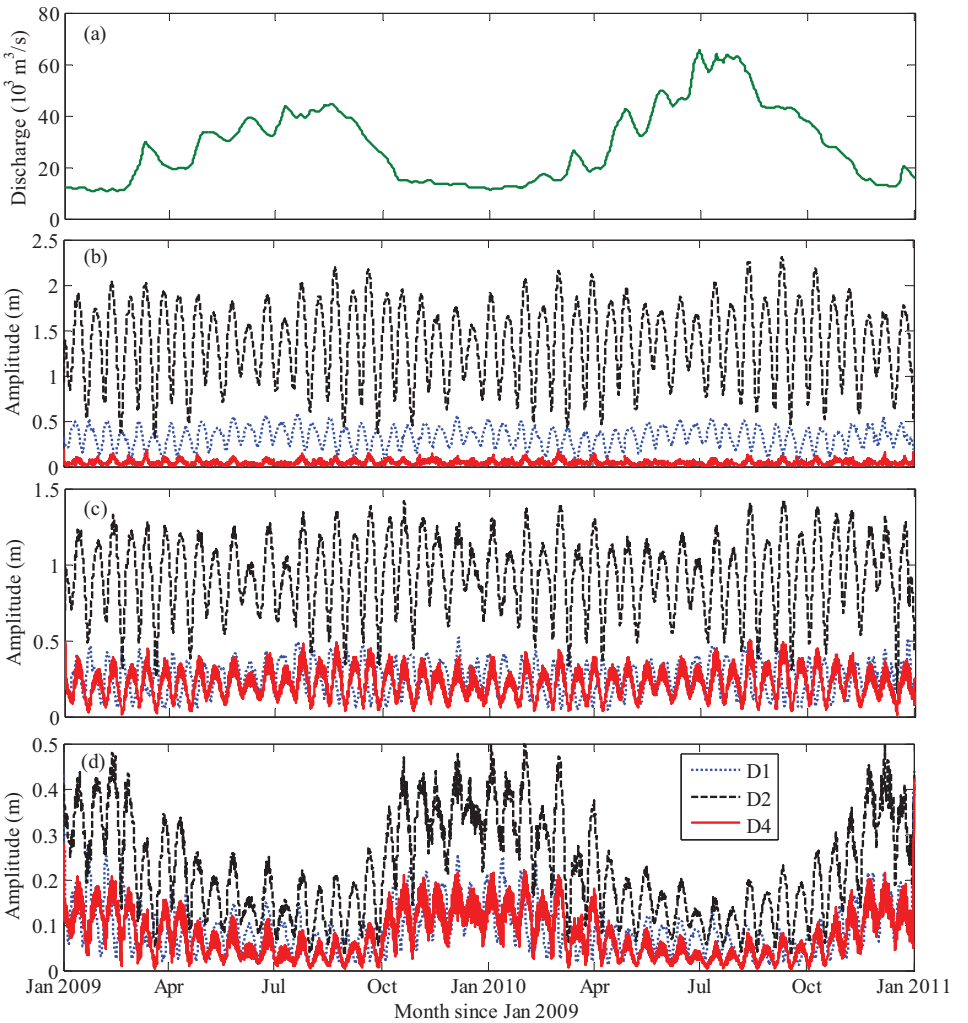

Figure 7. (a) River discharge at Datong; amplitudes of the diurnal (D_1), the semidiurnal (D_2), and the quarter-diurnal (D_4) tides at (b) Niupijiao, (c) Xuliujing, and (d) Nanjing for 2009 and 2010, determined by CWT analyses.

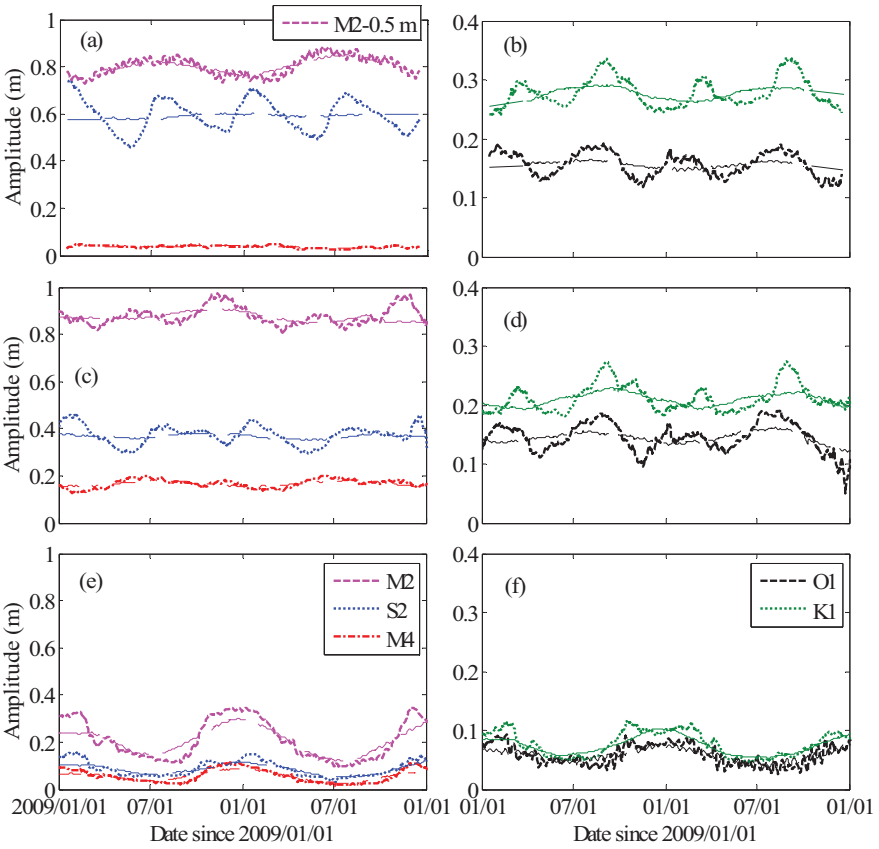

Figure 8. STHA-analyzed amplitudes of (a, c, e) semidiurnal tides M_2 and S_2 (including M_4 tide), and (b, d, f) diurnal tides O_1 and K_1 at (a, b) Niupijiao, (c, d) Xuliujing, and (e, f) Nanjing between 2009 and 2010. The thick lines indicate HA results from a 30 day window and the thin lines indicate results from a 180 day window. The M_2 amplitudes in Figure 8a are reduced by 0.5 m.

based tidal frequencies. At upriver stations, as suggested by Figure 6, much of the energy is not in tidal frequencies. The M_2 tide is the most significant constituent followed by the S_2 and N_2 tides in the D_2 band and the K_1 and O_1 tides in the D_1 band (Table 1). A diurnal to semidiurnal amplitude ratio $(A_{K1} + A_{O1} + A_{P1})/(A_{M2} + A_{S2} + A_{N2})$ is 0.24 at Niupijiao, indicating a mixed tidal regime. In the D_4 band, the M_4, MS_4, and MN_4 tides are of limited amplitudes at Niupijiao; however, their amplitudes increase landward to Yanglin (e.g., yearly averages of 0.20 m for the M_4 tide, and 0.16 m for the MS_4 tide) and then decrease farther upstream.

Low-frequency tides grow strongly in the upper portion of the YRE. For example, the fortnightly MSf tide (T = 14.8 days) is small at Niupijiao (0.026 m amplitude) but its amplitude increases profoundly to Xuliujing and further to Nanjing to ~0.20 m. Another fortnightly tide, Mf (T = 13.7 days), is overall less significant (e.g., 0.04 m at Nanjing), indicating the expected MSf dominance in the fortnightly frequency band. The monthly Mm tide (T = 27.6 days) also increase landward, though its absolute amplitude is smaller than the MSf tide (0.078 m at Nanjing). Semiannual and annual water level oscillations, reflected by Ssa and Sa tides, respectively, are considerable at Niupijiao (amplitudes of 0.04 m for Ssa and 0.17 m for Sa) and they reach large amplitudes at Nanjing (0.32 m for Ssa and 1.89 m for Sa; see Table 1). These calculated "Ssa" and "Sa" tides do not necessarily have an astronomical source. Near the ocean, they represent semiannual and annual MWL variations in the marginal East China Sea, where MWL can be ~0.5 m higher in summer (wet season) than in winter (dry season) due to varying solar radiation [*State Oceanic Administration of People's Republic of China (SOA)*, 2013]. Upriver, Ssa, and Sa represent increasing impact of the seasonally varying river discharges.

Use of a moving 31 days STHA resolves seasonally varying tidal amplitudes associated with river discharge fluctuations, unresolved tidal interactions and variations in oceanic input (Figure 8). For instance, at Nanjing, M_2 amplitude varies between 0.12 m in the wet season and 0.34 m in the dry season; S_2 amplitude varies

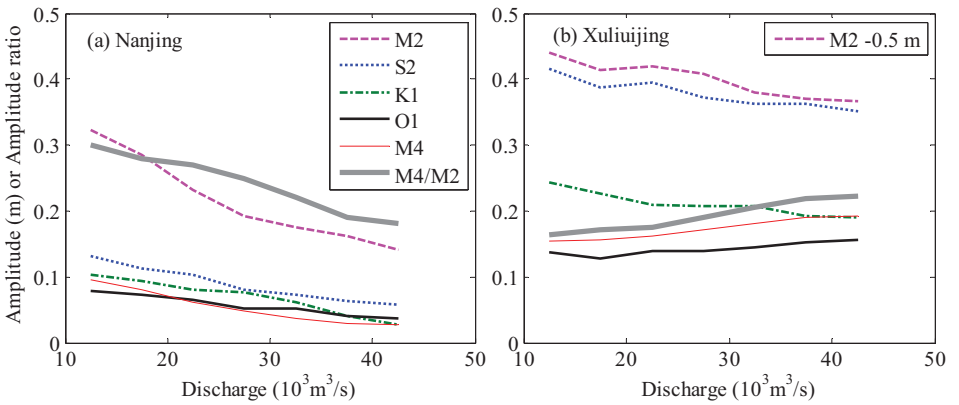

Figure 9. Variations of tidal amplitudes and A_{M4}/A_{M2} amplitude ratio (a) at Nanjing and (b) at Xuliujing with river discharges measured at Datong. The M_2 amplitude at Xuliujing in Figure 9b is reduced by 0.5 m. The central point of each discharge range is used with the tidal amplitudes, e.g., 12,500 m^3/s is used to represent the discharge range of 10,000–15,000 m^3/s.

between 0.04 and 0.15 m. This seasonal pattern is less evident downstream Xuliujing. Instead, semiannual variations of S_2, N_2, O_1, and K_1 tidal amplitudes become prominent at Xuliujing and Niupijiao. These seasonal variations are out of phase with the seasonal river discharge fluctuations. The semiannual variations reflect in part semiannual modulation of the oceanic tides, e.g., for O_1 that does not have substantial, neighboring constituent. They are also caused by constituents groupings that cannot be separated by STHA, e.g., the influences of unresolved constituents K_2 on S_2, Nu_2 on N_2, and P_1 on K_1 [*Amin*, 1985]. We note that the expected modulation of N_2 by Nu_2 is $<$20%, but the observed 6 month variations in N_2 are considerably larger.

A HA with a longer data window length (180 days) is used to resolve more tidal constituents, largely eliminating the effects of the unresolved constituents, though at the same time hides the modulations of tides by seasonally varying river discharge (Figure 8). The semiannual variations are generally smaller and more regular with the longer window (except at Nanjing because of strong river influence), though prominent semiannual variations remain, for example, for M_2 at Niupijiao. The later is presumably related to coastal processes at Niupijiao, and to a mix of coastal and fluvial processes elsewhere.

We then apply NSHA to interpret river discharge impacts on tidal constituents for river discharges between 10,000 and 45,000 m_3/s (Figure 9). M_2 amplitudes decrease at Nanjing from 0.33 m for a river discharge of 10,000–15,000 m^3/s to 0.14 m for a discharge of 40,000–45,000 m^3/s, consistent with STHA results. Similar trends are seen for most astronomical constituents at Nanjing and Xuliujing, but M_2 decays more rapidly with increasing river discharges at Nanjing (i.e., averagely 0.061 m/10,000 m^3/s) than at Xuliujing (i.e., averagely 0.025 m/10,000 m^3/s) as expected for a more landward station. The O_1 and M_4 tides behave differently at Xuliujing, where the O_1 and M_4 amplitudes increase slightly with increasing river discharges. Increasing O_1 amplitude may be attributed to energy transfer from M_2 and K_1 to O_1 through the M_2-O_1-K_1 triad interactions [*Parker*, 1991], though it is not obvious why K_1 and O_1 behave differently. Increasing M_4 tidal amplitude at Xuliujing for a high river discharge is consistent with HA and CWT results and consistent with energy transfer from M_2. Interestingly, the A_{M4}/A_{M2} amplitude ratio decreases at Nanjing (upriver) and increases at Xuliujing (downriver) with increasing river discharges. This phenomenon can be explained by river flow-enhanced tidal friction which has stronger effects in attenuating tidal amplitudes upriver but stronger effects in stimulating tidal wave distortion downriver (see section 4.2). In summary, NSHA results provide a valuable, quantitative perspective on the impact of river discharge on tidal properties.

3.4. Tidal Currents and Subtidal Friction

In this section, we relate subtidal water levels to variations in subtidal friction. Figure 10 shows the hourly tidal and daily averaged discharges at Xuliujing, together with daily discharge at Datong. The daily averaged tidal discharge at Xuliujing is coherent with the daily river discharge at Datong, aside from a short-time lag. Tidal elevation leads tidal discharge by about 70 min, indicating an essentially progressive tide. The ratios of flood tidal volume to ebb tidal volume at Xuliujing over a semidiurnal tidal cycle are about 0.6 and 0.1 in

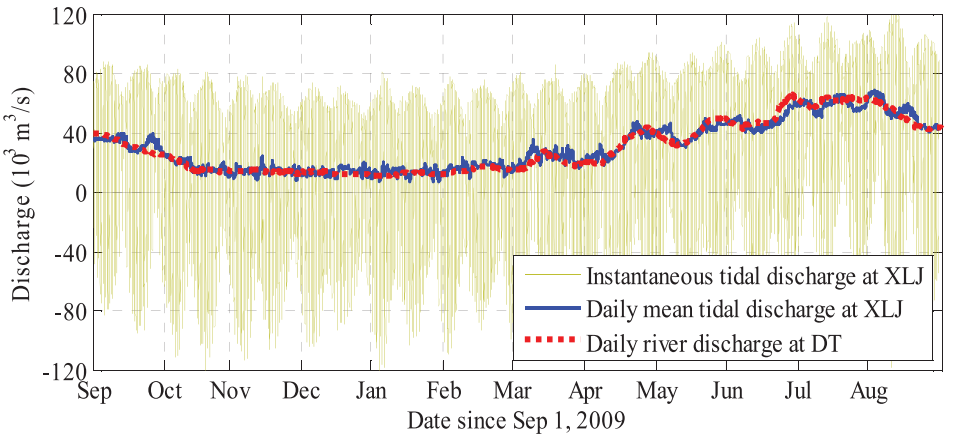

Figure 10. Daily river discharges at Datong (DT) and the instantaneous and daily tidal mean discharges at Xuliujing (XLJ) between September 2009 and August 2010. Negative values are in the landward direction.

the dry and wet seasons, respectively, reflecting seasonal variations in river discharge. Daily averaged discharge at Xuliujing shows limited fortnightly subtidal variations. This is because the subfrequency tidal discharge is at least an order of magnitude smaller than the mean daily discharges.

CWT analysis of tidal discharges shows wavelet power spectra in the D_1, D_2, and D_4 bands similar to these for the tidal water levels (Figure 11). D_4 tidal currents are significant at Xuliujing, but only limited energy in the low-frequency bands is detected, indicating a much less enriched frequency structure relative to tidal water levels. This confirms the limited subtidal discharge variations seen in Figure 10.

Cross-sectionally averaged tidal velocities provide dynamic insights into tidal water level variations (see Figure 12a). Ebb currents are overall larger than flood currents, but currents may reverse such that the peak

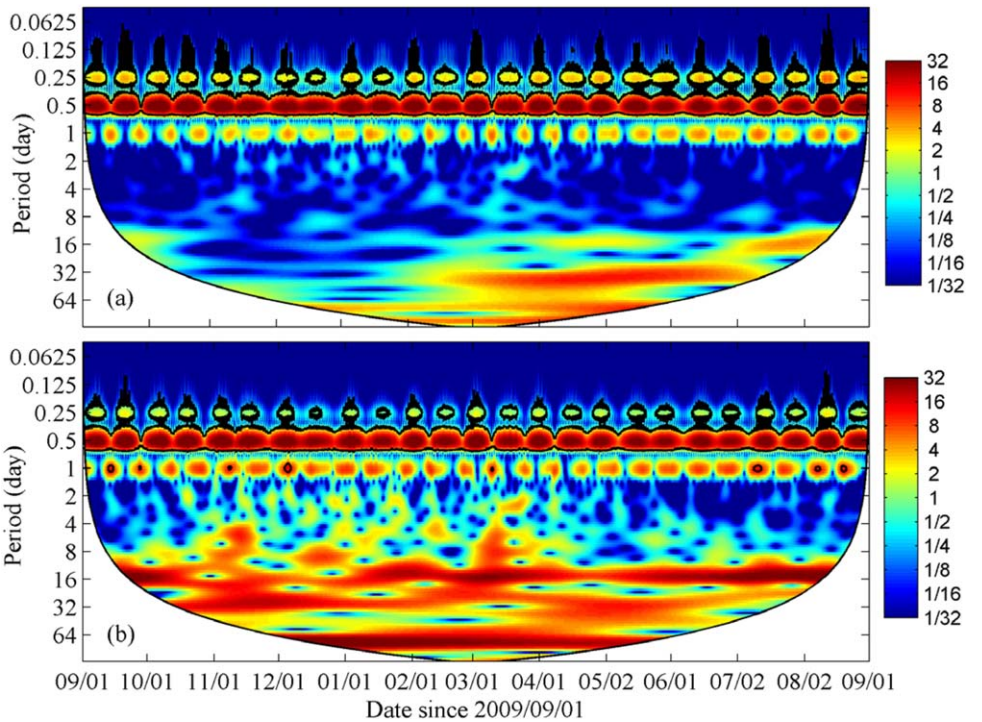

Figure 11. Wavelet power spectrum of (a) tidal discharge, (b) tidal water level at Xuliujing between 1 September 2009 and 31 August 2010. The original data are normalized to have unit energy at each frequency so the wavelet powers of tidal discharge and tidal water level have the same energy scales (see section 2.3). Other settings are the same as Figure 5.

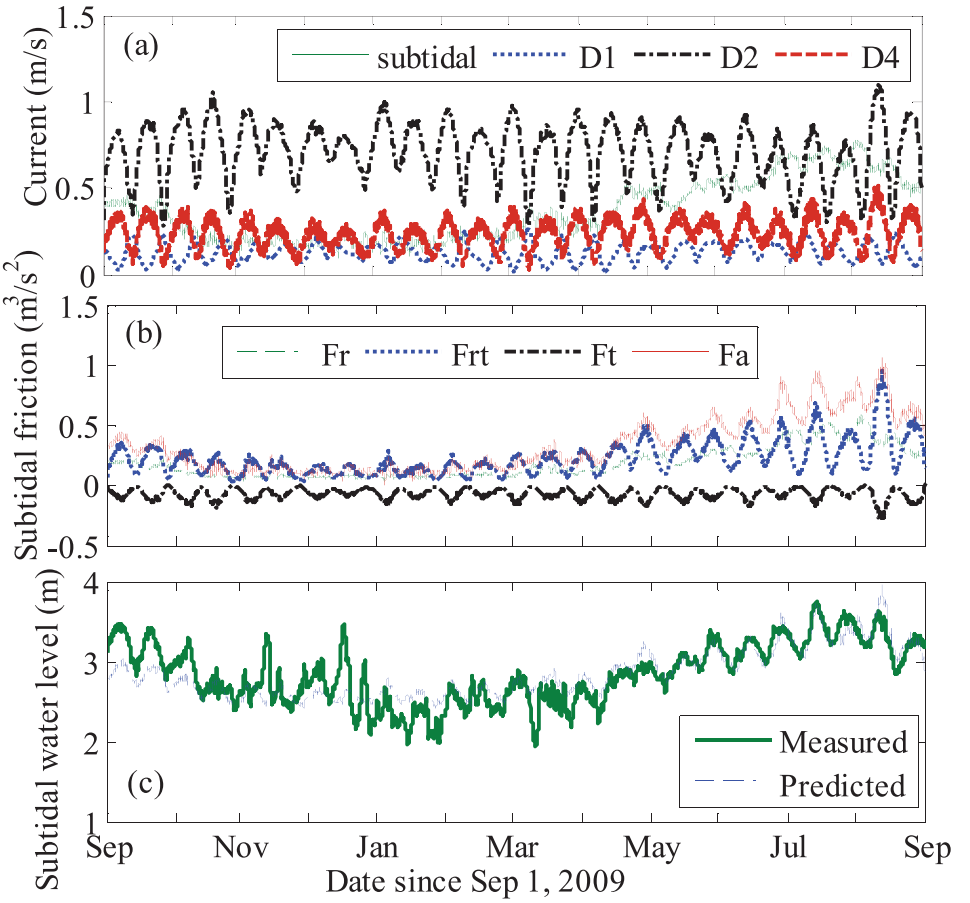

Figure 12. (a) Amplitudes of the D_1, D_2, and D_4 tidal currents, and the subtidal currents; (b) subtidal friction related to river flow (F_r), river-tide interaction (F_{rt}), and tidal asymmetry (F_t), and the total subtidal friction (F_a); (c) measured subtidal water levels and a prediction from a linear regression of F_a at Xuliujing between September 2009 and August 2010.

flood velocity is larger than peak ebb velocity in the dry season. Tidal current asymmetry is such that the ebb currents have a longer duration of high velocity, whereas flood currents have a shorter peak velocity duration. During the wet season and on neap tides, ebb currents can persist without reversal for a period of up to six semidiurnal cycles. Scale-averaged CWT analysis of tidal currents gives a time series of residual (subtidal) currents and currents for the D_1, D_2, and D_4 species (Figure 12a). Seasonal variations of subtidal current amplitudes are evident because of varying river discharges while the fortnightly, monthly, and semi-annual variations of the D_1, D_2, and D_4 current amplitudes are also prominent. The D_4 currents are even stronger than the D_1 currents, confirming the usual reasoning that the ratio of tidal current amplitude to tidal height amplitude increases with frequency.

We use the residual currents and currents of tidal species to estimate the contribution of river flow, river-tide interaction, and tidal asymmetry on subtidal friction according to equations (A6)–(A8). This calculation shows that river discharge and river-tide interaction are the dominant factors creating substantial subtidal friction, while the contribution of tidal asymmetry is minor and negative at Xuliujing (Figure 12b). The tidal asymmetry effect is negative because tidal wave distortion (faster high water propagation than low water) induces a flood-dominant tidal asymmetry. The tidal asymmetry term is relatively small because (1) D_1 tidal current amplitude is small, and (2) the D_2 and D_4 tides are nearly in quadrature with each other much of the year. In the dry season, river-tide interactions and tidal asymmetry have opposite signs and nearly cancel each other; thus, the contribution of river flow becomes significant in the balance.

The subtidal friction asymmetry between spring and neap tides explains the fortnightly subtidal water level variations. A linear regression between the total subtidal friction and the measured subtidal water levels at

Xuliujing has a skill of 0.62 (r^2). The predicted subtidal variations are in a good agreement with the measurements, indicating control of subtidal friction on subtidal water level variations (Figure 12c). Physically, this means that a higher subtidal friction on spring tides causes more water accumulation in the upstream region of the estuary, elevating MWL on spring tides. Tidal currents are stronger and there is more friction during spring tides than on neap tides; thus, spring tides are also damped faster than neap tides in the landward direction. The spring-neap variations of subtidal friction are in essence similar to the observation of larger friction for ebb currents than for flood currents in river-influenced estuaries. Also current prediction is more accurate during the wet season than the dry season in Figure 12c, because of river dominance of subtidal friction through both river flow and river-tide interaction in the wet season. It is expected that the effects of river flow are more dominant upstream, while tidal asymmetry and river-tide interaction are more prominent downstream, but currents are available only at a single location, so that this idea cannot be directly tested.

4. Discussion

4.1. Sources of Subtidal Variations

Nontidal forcing contributes to subfrequency tidal signals, causing tidalists to discard these constituents as contaminated by noise [*LeBlond*, 1991; *Jay and Flinchem*, 1997; *Denielson and Kowalik*, 2005; *Ray and Erofeeva*, 2014]. In the YRE, atmospheric and/or oceanic conditions are partly responsible for the monthly and semiannual variations in the tidal ranges (see Figures 4a and 7). The manifestation of surface tides by internal tides generated in the East China Sea may be an important contribution to the low-frequency variations in tides close to the coast, but future research is needed to quantify to what degree. Results in section 3.1 show that river discharge generates significant annual MWL variations and associated variations in tidal amplitudes, but limited variations in the fortnightly and monthly frequencies.

Tidal interactions are an important source of tidal monthly variations in tidal processes. The interaction of M_2 and S_2 causes spring-neap (fortnightly) variations in tidal properties; M_2 and N_2 interaction causes perigee-apogee (monthly) tidal variations. Since the M_2 tide is the dominant constituent in the YRE (e.g., 1.3 m at Niupijiao), an S_2 amplitude of 0.59 m could potentially cause a spring-neap tidal range difference of 2.36 m (about 2.21 m is detected from Figure 4a) at Niupijiao. Similarly, an N_2 amplitude of 0.23 m at Niupijiao is able to induce monthly maximum and minimum tidal range differences of 0.46 m (about 0.48 m detected from Figure 4a). Similar interactions occur between semidiurnal and diurnal tides (e.g., M_2 interacts with K_1). The tidal monthly variations in tidal ranges are also evident at Xuliujing but are dominated over by river-induced seasonal variations at Nanjing. It indicates spatially evolved tidal dynamics due to mixed coastal and fluvial processes in such a long system.

Tidal interactions also generate low-frequency tides. For instance, M_2-S_2 interaction generates an MSf tide (because of ω_{S2}-$\omega_{M2} = \omega_{MSf}$, where ω is tidal frequency), and M_2-N_2 interaction generates an Mm tide (because of ω_{M2}-$\omega_{N2} = \omega_{Mm}$). The generation of such compound tides reflects energy transfer from the principal bands to the subtidal bands [*Parker*, 1984; *Aubrey and Speer*, 1985; *Amin*, 1993]. Although tidal potential contains energy at the frequencies of MSf and Mm, this energy source is normally very limited and becomes negligible upriver [*LeBlond*, 1979]. HA results show that the MSf and Mm tides are small at Niupijiao and Datong, but gain significant energy in the central river, e.g., at Xuliujing and Nanjing. Cleary, fortnightly and monthly subtidal variations are dominantly created by frictional tidal interactions, mediated by river discharge but no directly by discharge.

CWT results indicate that the subtidal frequencies have their maximum amplitudes further upriver than the overtides. Larger MSf tidal amplitudes observed in the upstream parts of the Amazon and Columbia tidal rivers provide additional examples of this phenomenon [*Gallo and Vinzon*, 2005; *Jay et al*., 2014], which may be general in large tidal rivers. When the MSf amplitude grows to be the same order of the principal tides (i.e., about $S_2 + K_1$), the lowest low water level will be lower on neap tides than on spring tides, as observed at Nanjing. In that sense, lower MWL on neap tides than on spring tides can be interpreted as resulting from a forced fortnightly constituent.

That the amplitude maxima in the fortnightly and monthly tides are further landward than the maxima in the overtides has two causes. First, scaling arguments suggest that damping rate increases with frequency [*Godin*, 1999]. This idea applies directly only to linear tidal constituents that do not have an energy source

from frictional interaction in the tidal river, so that their amplitudes are controlled only by the balance between convergence and friction. It does emphasize, however, that internally generated overtide constituents cannot persist over long distances. The other reason is the fact that the fortnightly waves have a wavelength very much longer than the length of even a tidal river like the YRE and move through the system very slowly so that there is little or no phase variation along channel. Thus, the fortnightly waves should persist almost to the head of the tide, well landward of the point where overtide waves have almost disappeared.

4.2. River-Tide Interactions

River discharge has substantial effects on tidal dynamics by dissipating tidal energy, damping tidal amplitude, and altering tidal phases [*Godin*, 1985, 1999; *Jay*, 1991; *Jay and Flinchem*, 1997]. Theoretical analysis suggests that the amplitude of an incident wave from the ocean should vary in the landward direction with the square root of river discharge in a channel of constant width and depth [*Jay and Flinchem*, 1997], which leads to an approximately linear relationship between tidal damping modulus and river flow in the Columbia River estuary [*Kukulka and Jay*, 2003a]. The independent tidal damping effects by varying river discharge are, however, still poorly quantified because tidal damping is nonlocal; it is the integrated results of tidal wave propagation through a given channel geometry, and tidal decay is a nonlinear process. In this work we provide quantitative estimates of tidal amplitude variations under different river discharge conditions using NSHA (see Figure 8), which illustrates the impact of river discharges in causing tidal decay. It also emphasizes that the "harmonic constants" are not really constant over time in highly nonstationary river estuaries.

River discharge also modulates tidal interactions and the resultant generation of overtides and compound tides. This modulation is nicely reflected by enhanced M_4 generation at Xuliujing but reduced M_4 amplitudes at Nanjing during high flow periods. Though the absolute M_4 amplitudes are larger at Xuliujing than Nanjing, the M_4 tide has a larger amplitude and the A_{M4}/A_{M2} amplitude ratio is larger in the wet season downriver (e.g., at Xuliujing), whereas maximum M_4 amplitude and larger A_{M4}/A_{M2} amplitude ratio occur in the dry season upriver (e.g., at Nanjing). This suggests stronger tidal wave deformation upriver during the dry season but stronger tidal wave deformation downriver in the wet season. River discharge plays a significant role here by river-enhanced subtidal friction, which attenuates tidal energy upriver while stimulating energy transfer from the principal tides to overtides downriver.

Tides also influence outgoing river flow. River discharge induces MWL setup in the upstream region of an estuary (see Figure 3). A MWL rise up to 10 m at Datong in the YRE is beyond what a Stokes drift can explain, but can be partly seen as the "backwater effect" of the incoming tides exerting on the outgoing river flow.

4.3. Implications for River Tidal Dynamics

Low-frequency tidal processes partially explain subtidal water level variations. The lower lowest low waters occur on neap tides rather than on spring tides upstream Jiangyin in the YRE, because of the decayed of the principal tidal species with amplified subtidal frequencies upriver. For instance, at Nanjing, the MSf has an amplitude comparable with M_2 (see Table 1). The reversal of low waters between spring and neap tides can affect regional ecosystems and navigation channels; it thus deserves management attention. Furthermore, that the amplitude of the subtidal water level variations is comparable to that of the principal tides indicates a transition between fluvial and tidal dominance in the Yangtze tidal system. According to *Shen* [2003], Zhenjiang and Jiangyin are the locations where tidal currents cease to reverse in direction in the wet and dry seasons, respectively. Thus, following *Jay et al.* [2014], the subtidal phenomena can be used to define Jiangyin (or somewhere between Jiangyin and Zhenjiang) as an approximate boundary in the YRE between the tidal river (upstream) and the estuary (downstream). This division between tidal river and tidal estuary is of practical importance in that coastal and estuarine processes exert a dominant influence on tidal dynamics and associated sediment transport that persists hundreds km landward, before the river flow become the dominant influence on tidal oscillations further landward.

River-tide interactions also strongly affect tidal asymmetry. *Parker* [1984] observed landward increase in the A_{M4}/A_{M2} amplitude ratio along with damping of the M_2 tide in the Delaware estuary. *Lincoln and FitzGerald* [1988] noted a significant spring-to-neap decline in average tidal duration asymmetry between the rising

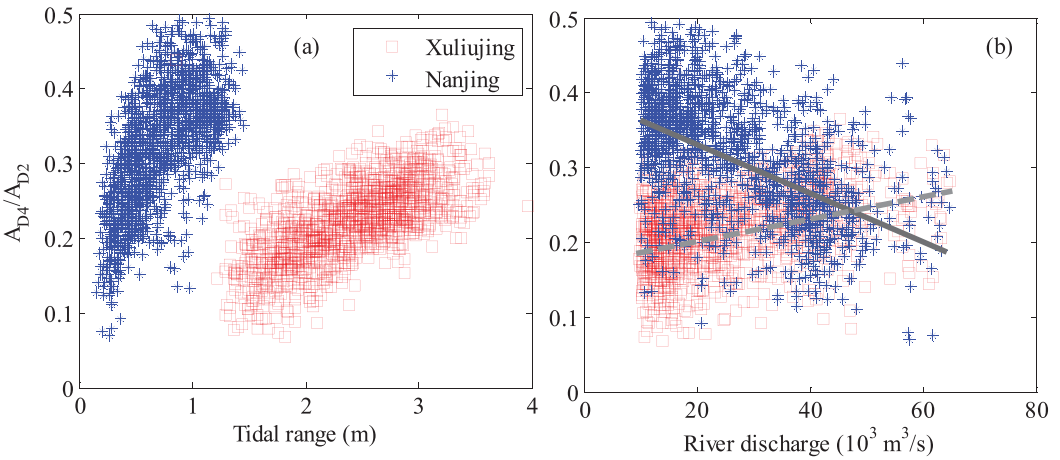

Figure 13. Relationships (a) between the A_{D4}/A_{D2} tidal amplitude ratio and tidal range and (b) between A_{D4}/A_{D2} ratio and river discharge at Datong, at Nanjing (blue stars) and Xuliujing (red squares) based on CWT analysis of tidal water levels between 2006 and 2013. The solid lines in Figure 13b indicate result from linear regression.

and falling tides. *Speer et al*. [1991] found that the magnitude of tidal distortion increased with increasing D_2 amplitude or decreasing mean tidal level. *Wang et al*. [1999] further confirmed that tidal asymmetry is stronger on spring tides than on neap tides. In this work, we found larger A_{D4}/A_{D2} amplitude ratios (determined by CWT) on spring tides than on neap tides both at Nanjing and Xuliujing (Figure 13a). The A_{D4}/A_{D2} amplitude ratios are also larger at Nanjing than at Xuliujing in the dry season (Figure 13b), suggesting that the D_2 tidal energy is increasingly transferred to the D_4 band upriver, though the tides are overall more damped therein. The variations of A_{D4}/A_{D2} are correlated with the A_{M4}/A_{M2} ratios (Figure 9), confirming the nonlinear behavior of quarter-diurnal tide in response to increased river discharges.

The nonlinear M_4 tide and its associated tidal asymmetry is one of the dominant mechanisms generating residual sediment transport in many systems [*Dronkers*, 1986], but river flow in the YRE is so strong that the effects of tide-induced asymmetric currents on residual sediment transport are limited compared to flow-enhanced, ebb-directed sediment transport [*Guo et al*., 2014]. However, tidal interactions and the resultant tidal asymmetry are still important in that they cause fluctuations in bed friction and water levels that have impacts on navigation and ecosystems.

The instantaneous response of YRE tides to time-varying river discharges is still not fully resolved by available HA and CWT techniques and new methods are needed. As one potentially useful approach, *Matte et al*. [2013] generalized HA by modifying the basis functions used in T_TIDE [*Pawlowicz et al*., 2002] to reflect the impact of nonstationary river flow based on *Jay* [1991] and *Kukulka and Jay* [2003a, 2003b]. In this NS_TIDE approach, the tidal "constants" of HA are modified so that they are low-order polynomial functions of river flow and ocean tidal ranges. Thus, the output of NS_TIDE is a time series of amplitudes and phases of tidal constituents. NS_TIDE attempts to provide the merits of HA and CWT and at the same time overcomes their defects. First applications of NS_TIDE method in the Columbia River estuary [*Matte et al*., 2013] and the St. Lawrence estuary [*Matte et al*., 2014] show that it can be a useful tool in analyzing and understanding nonstationary tidal signals. Further application of NS_TIDE to the strongly variable river flow seen in the YRE could help to validate the usefulness of NS_TIDE as well as elucidating YRE tidal dynamics.

5. Conclusions

We have explored nonstationary and nonlinear tidal dynamics based on tidal analysis in the YRE. We have applied HA and CWT methods to multiple time series of water levels to resolve tidal species and constituents. Tidal height and CWT analyses reveal significant subtidal variations in tidal water levels, tidal ranges, and tidal amplitudes. Tidal fortnightly and monthly variations in water levels are largely explained by flow-enhanced tidal interactions between astronomical constituents that generating subtidal motions. Nontidal forcing, herein river discharge and probably oceanic internal tides, induces oscillations with semiannual and annual frequencies. Semiannual variations in major tidal constituents that are out of phase with seasonal

river discharge variations occur near the river mouth and remains to be explained. MWL is observed to be lower on neap tides than on spring tides in a large portion of the estuary (upstream Wusong) because of enhanced generation of fortnightly tidal waves. The lowest water levels are lower on neap tides in the tidal river portion (upstream Jiangyin) because the amplitude of the fortnightly waves becomes comparable with the damped astronomical tides landward of this point. Based on the significance of the fortnightly tides, we suggest a division around Jiangyin (km-405) to distinguish a tidal river portion and tidal estuary portion in the Yangtze tidal system.

CWT analyses reveal strong time-varying tidal damping of principal tides along with spatial evolution of the tidal spectrum. Both the sub and supratidal frequencies are of limited amplitude at the coast, but are substantial and exhibit strong spatial variability in the estuary. The A_{M4}/A_{M2} and A_{D4}/A_{D2} amplitude ratios are larger upriver in the dry season and larger downriver in the wet season, indicating that nonlinear M_4 tidal distortion varies with river discharges. That is, M_4 amplitude represents a balance between generation from M_2 and decay due to river flow, and higher river discharge push the point of maximum M_4 amplitude downriver. A decomposition of subtidal friction suggests that river flow and river-tide interaction are the major contribution to subtidal friction and associated fortnightly subtidal water level variations. Overall, river discharge plays a substantial role in controlling tidal interactions by dissipating the principal (linear) tidal constituents and stimulating tidal energy transfer from the principal bands to the lower and higher frequencies.

The HA and CWT results are consistent with each other and combined usage of them reveals nonstationary and nonlinear nature of river tidal dynamics, providing perspectives on river-tide dynamics. NSHA is shown to be a useful technique for analyzing tidal-fluvial interactions, but it has limitations related to the disparate sections of data analyzed within any each discharge range, and a lack of distinction between rising and falling hydrographs.

Understanding river tidal dynamics and river-tide interactions has important implications for tidal prediction and for managing estuarine ecosystem services. Intensified regulation of river discharge processes by dams in the Yangtze River basin and the potential impact of climate change on river flow will impose further alternation on the river tidal dynamics. More and better water level and current data are needed to infer detailed along-channel evolution of the tidal frequency structure. Also, the behavior of the tidal monthly and seasonal variations need further study, for example to differentiate the effects of coastal processes like internal tides from nontidal forcing by river flow.

Appendix A: Theory of Harmonic Analysis (HA), Continuous Wavelet Transform (CWT), and Subtidal Friction Decomposition

One method we use in this study to analyze water levels is the HA [*Godin*, 1972; *Pawlowicz et al*., 2002]. The HA method, a least squares fitting procedure applied to finite segment of data, considers a water level time series as a sum of a mean and a number of harmonic terms appropriate to the record length and sampling interval, as follows:

$$H(t)=b_o(t)+\sum_{n=1}^{N}[A_n\cos(\omega_n t-\Phi_n)]+r(t), \tag{A1}$$

in which t is time; H represents the measured time series of water levels; $b_o(t)$ is MWL; A, ω, and Φ are tidal amplitude, frequency, and phase, respectively, of tidal constituents n ($n = 1,2...N$); $r(t)$ represents the residual components. Details of the method and the programming are referred to *Godin* [1972] and *Pawlowicz et al*. [2002].

Note that frequency resolution of HA increases with increasing the time series length. For instance, a window length of 30 days resolves 29 constituents (excluding subfrequency constituents such as MSf and Mm). But a 30 day HA (short-term HA, STHA) does not resolve closely spaced constituents like K_1 and P_1, and S_2 and K_2. In the widely applied T_TIDE function, P_1 and K_2 tides are solved by inference relationships from K_1 and S_2 tides, respectively [*Pawlowicz et al*., 2002].

The CWT method is used to analyze time series of signals containing nonstationary power at different frequencies. *Farge* [1992] and *Daubechies* [1992] provided a general introduction of the (continuous) wavelet

transformation, and *Torrence and Compo* [1998], *Grinsted et al*. [2004], *Jay and Flinchem* [1997], and *Flinchem and Jay* [2000] presented applications of CWT in geophysical and oceanographic studies. The idea of CWT is to apply a wavelet transform as a band-pass filter to a time series of tidal signals. The CWT $W_t(s)$ (m) determined using scaled and normalized wavelets is defined as a convolution of a time series of signal $H(t)$ ($t = 1, 2. . .M$):

$$W_k(s) = \sqrt{\frac{\delta t}{s}} \sum_{k'=1}^{M} H_{k'} \psi\left[(k'-k)\frac{\delta t}{s}\right], \tag{A2}$$

where s is the scale (or frequency); k and k' are time series; δt is the uniform time step (1 h in this study), and M is the length of the time series; ψ is a normalized wavelet function that has unit energy at each scale s. Normalization of wavelet function is enforced to ensure that the wavelet transforms are directly comparable to each other at each scale. Then the wavelet amplitude $|W_k(s)|$ and wavelet power $|W_k(s)|^2$ are estimated by varying the wavelet scale s and translating along the localized time k. Data gap in $H(t)$ is filled by NaN value in the CWT analysis.

A CWT requires a wavelet function (symmetric in its real and asymmetric in its imaginary parts) whose form and scale are optimized for tidal analysis. The choice of wavelet function and its scale is crucial for adequate results. Here we employ a prototype Morlet function as that used by *Torrence and Compo* [1998] and *Sassi and Hoitink* [2013]. The Morlet wavelet is nicely applicable for tidal signals because it satisfies the admissibility condition (i.e., the wavelet oscillates to have its mean value equal to zero) [*Daubechies*, 1992; *Farge*, 1992] and its wavelet scale (when $\omega_o = 6$) is almost equal to the Fourier period [*Torrence and Compo*, 1998]. The Morlet wavelet function reads as

$$\psi(\gamma) = \pi^{-1/4} e^{i\omega_o \gamma} e^{-\frac{1}{2}\gamma^2}, \tag{A3}$$

where ω_o is dimensionless frequency and γ is dimensionless time. ω_o is set to 6 here for tidal analysis because it provides a good balance between time and frequency resolution [*Grinsted et al*., 2004].

In essence, the CWT transforms a time series water levels in a manner somewhat similar to a Fourier transform. But the one-dimensional input is transformed into a two-dimensional output in time frequency; thus, one is able to determine both the dominant frequency mode and the variations of this mode over time [*Jay and Flinchem*, 1997; *Torrence and Compo*, 1998]. We can check the performance of CWT by reconstructing a time series of signal based on the following equation [*Torrence and Compo*, 1998]:

$$H_k = \frac{\delta j \sqrt{\delta t}}{C_\delta \pi^{-1/4}} \sum_{j=0}^{J} \frac{R\{W_k(s_j)\}}{\sqrt{s_j}}, \tag{A4}$$

where δj is scale step (0.1 in this study thus indicating 10 scales per octave); δt is the time step in the original data; C_δ is a constant factor (value of 0.776) for the Morlet wavelet; J is the total number of scales; $R\{\cdot\}$ indicates the real part of the complex wavelet transform. Preliminary analyses showed that the CWT performed quite well by giving a mean squared error of 0.67 cm on 3 years' data (2008–2010) at Xuliujing in the YRE, for example, indicating the selection of wavelet and scale step to be reasonable.

The amplitude of each discrete scale is obtained by a normalization correction to $|W_k(s)|$. Since the scales in CWT analyses are not exactly coincidently identical to the frequencies of tidal constituents, the CWT analysis abandons astronomical tidal constituents (e.g., M_2 and S_2 in the semidiurnal band; O_1 and K_1 in the diurnal band). Instead, we calculate amplitudes of the physical tidal species (e.g., the diurnal, semidiurnal and quarter-diurnal bands, namely D_1, D_2, and D_4, respectively here) by integrating wavelet power in the diurnal, semidiurnal and quarter-diurnal frequency bands and converting them into wavelet amplitude, as follows:

$$A_{Di} = \sqrt{\int_{s_1^i}^{s_2^i} \frac{s}{\delta t} |W(s)|^2 ds / s_{Di}}, \tag{A5}$$

where A_{Di} is the amplitude of tidal species D_i ($i = 1, 2, 4$); s_{Di} is the predetermined scale of tidal species D_i, e.g., $s_{D2} = 0.5$ cpd; s_1^i and s_2^i are the lower and upper bound of the scale range of the tidal species D_i. Specifically, the diurnal (D_1) amplitude integrates frequency from 0.8991 to 1.1678 cycles per day (cpd); the

semidiurnal (D_2) amplitude integrates frequency from 0.4740 to 0.5680 cpd; and the quarterdiurnal (D_4) amplitude integrates frequency from 0.2455 to 0.2683 cpd. These frequency boundaries are selected based on the known tidal spectrum, for example 0.8991 and 1.1678 cpd can represent the lowest and highest frequencies in the diurnal tidal band, respectively.

One constraint of CWT is that the wavelet-frequency resolution decreases as scale decreases and time resolution increases. There is a trade-off between time and frequency uncertainties embodied in the Heisenberg uncertainty principle [*Jay and Flinchem*, 1997; *Torrence and Compo*, 1998]. There are also increasing edge effects for longer wavelets (lower frequencies) at both ends of a time series [*Torrence and Compo*, 1998; *Grinsted et al*., 2004]. These factors suggest that a longer time series of data is preferred, especially for lower frequency signals. Nonetheless, a CWT analysis nicely illustrates the adjustment of river tides to rapid river discharge variations. Thus, it is an effective method to analyze nonstationary tidal signals.

The detected subtidal behavior are explained by subtidal friction variations based on a total current decomposition by $U = u_0 + u_1\cos(\omega_1 t + \varnothing_1) + u_2\cos(\omega_2 t + \varnothing_2) + u_4\cos(\omega_4 t + \varnothing_4)$ and an approximation of the quadratic friction by $U|U| \approx aU + bU^3$. Integration of the friction term over a diurnal tidal cycle leads to three subtidal friction terms remained [*Buschman et al*., 2009], as follows:

$$F_r = aU_0 + bU_0^3, \tag{A6}$$

$$F_{rt} = 1.5bU_0(U_1^2 + U_2^2 + U_4^2), \tag{A7}$$

$$F_t = 0.75b[U_1^2U_2\cos(2\phi_1 - \phi_2) + U_2^2U_4\cos(2\phi_2 - \phi_4)], \tag{A8}$$

where U is velocity (m/s) with subscripts 0, 1, 2, 4 indicating subtidal currents, D_1, D_2, and D_4 tidal currents, respectively. The $\varnothing_i$ are phases of the D_1, D_2, and D_4 tidal currents. The D_i and $\varnothing_i$ (i = 1, 2, 4) are derived from CWT analysis of the measured time series tidal currents. The constants a and b are set to 0.3395 and 0.6791, respectively, following *Godin* [1999]. The *Dronkers* [1964] cubic Tschebyschev polynomial decomposition of $U|U|$ (used by *Kukulka and Jay* [2003a]) leads to very similar results, except that the coefficients vary with the ratio of river flow to total velocity. Overall, equations (A6)–(A8) indicates that subtidal variations of tidal currents induce variations in subtidal friction, which cause subtidal water level fluctuations.

Acknowledgments

River discharge and water level data were collected from the bureau of hydrology, Changjiang Water Resources Commission (http://xxfb.hydroinfo.gov.cn/ssIndex.html). This study was funded by National Science Foundation of China (grants 41276080 and 51320105005), the Foundation of Science and Technology Commission of Shanghai Municipality (grant 12230707500), and the Non-profit Industry Financial Program of Ministry of Water Resources China (grant 201201070-03). We also thank the China Scholarship Council (CSC) (grant 2009101208) and the ReSeDUE project (grant 60038881) for sponsoring the first author for the study in Delft. Funding to D. A. Jay was provided by US National Science Foundation (grant OCE-0929055). Discussions with Maximiliano Sassi (NIOZ) were appreciated. Comments from the anonymous reviewers and the Editors are also thanked.

References

Amin, M. (1985), Temporal variations of tides on the west coast of Great Britain, *Geophys. J. R. Astron. Soc.*, *82*, 279–299.

Amin, M. (1993), The mutual influence of tidal constituents in the presence of bottom stress, *Estuarine Coastal Shelf Sci.*, *37*, 625–633.

Aubrey, D. G., and P. E. Speer (1985), A study of non-linear tidal propagation in shallow inlet/estuarine systems Part I: Observations, *Estuarine Coastal Shelf Sci.*, *21*, 185–205.

Buschman, F. A., A. J. F. Hoitink, M. van der Vegt, and P. Hoekstra (2009), Subtidal water level variation controlled by river flow and tides, *Water Resour. Res.*, *45*, W10420, doi:10.1029/2009WR008167.

Cai, H. Y., H. H. G. Savenije, Q. S. Yang, S. Y. Ou, and Y. P. Lei (2012), Influence of river discharge and dredging on tidal wave propagation: Modaomen Estuary case, *J. Hydraul. Eng.*, *138*, 885–896.

Darwin, G. H. (1891), Bakerian lectures: On tidal prediction, *Philos. Trans. R. Soc. London A*, *182*, 159–229.

Daubechies, I. (1992), *Ten Lectures on Wavelets*, Soc. for Ind. and Appl. Math., Philadelphia, Pa.

Dean, R. G. (1966), Tides and harmonic analysis, in *Estuary and Coastline Hydrodynamics*, edited by A. T. Ippen, pp. 197–229, McGraw-Hill, N. Y.

Denielson, S., and Z. Kowalik (2005), Tidal currents in the St. Lawrence Island region, *J. Geophys. Res.*, *110*, C10004, doi:10.1029/2004JC002463.

Doodson, A. T. (1921), The harmonic development of the tide-generating potential, *Proc. R. Soc. London, Ser. A*, *100*, 305–329.

Dronkers, J. J. (1964), *Tidal Computations in Rivers and Coastal Waters*, pp. 219–304, North-Holland, Amsterdam.

Dronkers, J. J. (1986), Tidal asymmetry and estuarine morphology, *Neth. J. Sea Res.*, *20*(2/3), 117–131.

Farge, M. (1992), Wavelet transforms and their application to turbulence, *Annu. Rev. Fluid Mech.*, *24*, 395–457.

Flinchem, E. P., and D. A. Jay (2000), An introduction to wavelet transform tidal analysis methods, *Estuarine Coastal Shelf Sci.*, *51*, 177–200.

Foreman, M. G. G. (1977), Manual for tidal heights analysis and prediction, *Pac. Mar. Sci. Rep.*, *77–10*, 58 pp..

Foreman, M. G. G., W. R. Grawford, and R. F. Marsden (1995), De-tiding: Theory and practice, in *Quantitative Skill Assessment for Coastal Ocean Models, Coastal Estuarine Stud.*, vol. 47, edited by D. R. Lynch and A. M. Davies, pp. 203–239, AGU, Washington, D. C.

Foreman, M. G. G., J. Y. Cherniawsky, and V. A. Ballantyne (2009), Versatile harmonic tidal analysis: Improvements and applications, *J. Atmos. Oceanic Technol.*, *26*, 806–817.

Friedrichs, C. T., and D. G. Aubrey (1988), Non-linear tidal distortion in shallow well-mixed estuaries: A synthesis, *Estuarine Coastal Shelf Sci.*, *27*, 521–545.

Friedrichs, C. T., and D. G. Aubrey (1994), Tidal propagation in strongly convergent channels, *J. Geophys. Res.*, *99*, 3321–3336.

Frison, T. W., M. D. Earle, H. D. I. Abanel, and W. D. Scherer (1999), Interstation prediction of ocean water levels using methods of nonlinear dynamics, *J. Geophys. Res.*, *104*, 13,653–13,666, doi:10.1029/1999JC900025.

Gallo, M. N., and S. B. Vinzon (2005), Generation of overtides and compound tides in the Amazon estuary, *Ocean Dyn.*, *55*, 441–448.

Gao, B., D. Yang, and H. Yang (2013), Impact of the Three Gorges Dam on flow regime in the middle and lower Yangtze River, *Quat. Int.*, *304*, 43–50.
Godin, G. (1972), *The Analysis of Tides*, Univ. of Toronto Press, Buffalo, 264 pp.
Godin, G. (1983), The spectra of point measurements of currents: Their features and their interpretations, *Atmos. Ocean*, *21*(3), 263–284.
Godin, G. (1985), Modification of river tides by the discharge, *J. Waterw. Port Coastal Ocean Eng.*, *111*(2), 257–274.
Godin, G. (1991), Frictional effects in river tides, in *Tidal Hydrodynamics*, edited by B. B. Parker, pp. 379–402, John Wiley, Toronto, Canada.
Godin, G. (1999), The propagation of tides up rivers with special consideration of the upper Saint Lawrence River, *Estuarine Coastal Shelf Sci.*, *48*, 307–324.
Grinsted, A., J. C. Moore, and S. Jevrejeva (2004), Application of the cross wavelet transform and wavelet coherence to geophysical time series, *Nonlinear Processes Geophys.*, *11*(5–6), 561–566.
Guo, L. C., M. van der Wegen, J. A. Roelvink, and Q. He (2014), The role of river flow and tidal asymmetry on 1D estuarine morphodynamics, *J. Geophys. Res. Earth Surf.*, *119*, 2315–2334, doi:10.1002/2014JF003110.
Hoitink, A. J. F., F. A. Buschman, and B. Vermeulen (2009), Continuous measurements of discharge from a horizontal acoustic Doppler current profiler in a tidal river, *Water Resour. Res.*, *45*, W11406, doi:10.1029/2009WR007791.
Horrevoets, A. C., H. H. G. Savenije, J. N. Schuurman, and S. Graas (2004), The influence of river discharge on tidal damping in alluvial estuaries, *J. Hydrol.*, *294*, 213–228.
Jay, D. A. (1991), Green's law revisited: Tidal long-wave propagation in channels with strong topography, *J. Geophys. Res.*, *96*, 20,585–20,598.
Jay, D. A., and E. P. Flinchem (1997), Interaction of fluctuating river flow with a barotropic tide: A demonstration of wavelet tidal analysis methods, *J. Geophys. Res.*, *102*, 5705–5720.
Jay, D. A., and E. P. Flinchem (1999), A comparison of methods for analysis of tidal records containing multi-scale non-tidal background energy, *Cont. Shelf Res.*, *19*, 1695–1732.
Jay, D. A., and T. Kukulka (2003), Revising the paradigm of tidal analysis—The use of non-stationary data, *Ocean Dyn.*, *53*, 110–125.
Jay, D. A., B. S. Giese, and C. R. Sherwood (1990), Energetics and sedimentary processes in the Columbia River Estuary, *Prog. Oceanogr.*, *25*, 157–174.
Jay, D. A., K. Leffler, H. L. Diefenderfer, and A. B. Borde (2014), Tidal-fluvial and estuarine processes in the lower Columbia River: I. Along-channel water level variations, Pacific Ocean to Bonneville Dam, *Estuaries Coasts*, *38*, 415–433, doi.10.1007/s12237.014–8919-0.
Kukulka, T., and D. A. Jay (2003a), Impacts of Columbia River discharge on salmonid habitat: 1. A non-stationary fluvial tide model, *J. Geophys. Res.*, *108*(C9), 3293, doi:10.1029/2002JC001382.
Kukulka, T., and D. A. Jay (2003b), Impacts of Columbia River discharge on salmonid habitat: 2. Changes in shallow-water habitat, *J. Geophys. Res.*, *108*(C9), 3294, doi:10.1029/2003JC001829.
Lanzoni, S., and G. Seminara (1998), On tide propagation in convergent estuaries, *J. Geophys. Res.*, *103*, 30,793–30,812.
LeBlond, P. H. (1978), On tidal propagation in shallow rivers, *J. Geophys. Res.*, *83*, 4717–4721.
LeBlond, P. H. (1979), Forced fortnightly tides in shallow rivers, *Atmos. Ocean*, *17*(3), 253–264.
LeBlond, P. H. (1991), *Tides and their interactions with other oceanographic phenomena in shallow water (review)*, in Tidal Hydrodynamics, edited by B. B. Parker, pp. 357–378.
Leffler, K. E., and D. A. Jay (2009), Enhancing tidal harmonic analysis: Robust (hybrid L^1/L^2) solutions, *Cont. Shelf Res.*, *29*, 78–88.
Le Provost, C. (1991), Generation of overtides and compound tides (review), in *Tidal Hydrodynamics*, edited by B. B. Parker, pp. 269–295, John Wiley, Toronto, Canada.
Li, C. Y., and J. O'Donnell (2005), The effect of channel length on the residual circulation in tidally dominated channels, *J. Phys. Oceanogr.*, *35*, 1826–1840.
Lien, R.-C., T. B. Sanford, S. Jan, M. H. Chang, and B. B. Ma (2013), Internal tides on the East China Sea continental slope, *J. Mar. Res.*, *71*, 151–185.
Lincoln, J. M., and D. M. FitzGerald (1988), Tidal distortion and flood dominance at five small tidal inlets in southern Maine, *Mar. Geol.*, *82*, 133–148.
Matte, P., D. A. Jay, and E. D. Zaron (2013), Adaptation of classical tidal harmonic analysis to nonstationary tides, with application to river tides, *J. Atmos. Oceanic Technol.*, *30*(3), 569–589.
Matte, P., Y. Secretan, and J. Morin (2014), Temporal and spatial variability of tidal-fluvial dynamics in the St. Lawrence fluvial estuary: An application of nonstationary tidal harmonic analysis, *J. Geophys. Res.*, *119*, 5724–5744, doi:10.1002/2014JC009791.
Parker, B. B. (1984), Frictional effects on tidal dynamics of shallow estuary, PhD dissertation, 291 pp., Johns Hopkins Univ. Press, Baltimore, Md.
Parker, B. B. (1991), The relative importance of the various nonlinear mechanisms in a wide range of tidal interactions, in *Tidal Hydrodynamics*, edited by B. B. Parker, pp. 237–268, John Wiley, Toronto, Canada.
Pawlowicz, R., B. Beardsley, and S. Lentz (2002), Classical tidal harmonic analysis including error estimates in MATLAB using T_TIDE, *Comput. Geosci.*, *28*, 929–937.
Pugh, D. T. (1987), *Tides, Surges and Mean Sea-Level*, 472 pp., John Wiley, Hoboken, N. J.
Ray, R. D., and S. Y. Erofeeva (2014), Long-period tidal variations in the length of day, *J. Geophys. Res. Solid Earth*, *119*, 1498–1509, doi: 10.1002/2013JB010830.
Sassi, M. G., and A. J. F. Hoitink (2013), River flow controls on tides and tide-mean water level profiles in a tidal freshwater river, *J. Geophys. Res. Oceans*, *118*, 4139–4151, doi:10.1002/jgrc.20297.
Savenije, H. H. G. (2005), *Salinity and Tides in Alluvial Estuaries*, Elsevier Sci., Amsterdam.
Savenije, H. H. G., M. Toffolon, J. Haas, and E. J. M. Veling (2008), Analytical description of tidal dynamics in convergent estuaries, *J. Geophys. Res.*, *113*, C10025, doi:10.1029/2007JC004408.
Shen, H. T. (Ed.) (2003), *Saltwater Intrusion in the Changjiang Estuary* [in Chinese], China Ocean Press, Beijing.
Shetye, S. R., and V. Vijith (2013), Sub-tidal water-level oscillations in the Mandovi estuary, west coast of India, *Estuarine Coastal Shelf Sci.*, *134*, 1–10.
Simon, B. (1991), The species concordance method of tidal prediction, in *Tidal Hydrodynamics*, edited by B. B. Parker, pp. 725–736, John Wiley, Toronto, Canada.
Song, D. H., X. H. Wang, A. E. Kiss, and X. W. Bao (2011), The contribution of tidal asymmetry by different combinations of tidal constituents, *J. Geophys. Res.*, *116*, C12007, doi:10.1029/2011JC007270.
Speer, P. E., and D. G. Aubrey (1985), A study of non-linear tidal propagation in shallow inlet/estuarine systems Part II: Theory, *Estuarine Coastal Shelf Sci.*, *21*, 207–224.

Speer, P. E., D. G. Aubrey, and C. T. Friedrichs (1991), Non-linear hydrodynamics of shallow tidal inlet/bay systems, in *Tidal Hydrodynamics*, edited by B. B. Parker, pp. 321–339, John Wiley, Toronto, Canada.

State Oceanic Administration of People's Republic of China (SOA) (2013), *China Sea Level Bulletins 2013*, Ocean Press, Beijing.

Torrence, C., and G. P. Compo (1998), A practical guide to wavelet analysis, *Bull. Am. Meteorol. Soc.*, *79*(1), 61–78.

van Rijn, L. C. (2011), Analytical and numerical analysis of tides and salinities in estuaries; part I: Tidal wave propagation in convergent estuaries, *Ocean Dyn.*, *61*, 1719–1741.

Walters, R. A., and R. E. Werner (1991), Nonlinear generation of overtides, compound tides, and residuals, in *Tidal Hydrodynamics*, edited by B. B. Parker, pp. 297–320, John Wiley, Toronto, Canada.

Wang, Z. B., C. Jeuken, and H. J. de Vriend (1999), Tidal asymmetry and residual sediment transport in estuaries, *WL Hydraul. Rep., Z2749*, 66 pp.

Yun, C. X. (2004), *Recent Evolution of the Yangtze Estuary and Its Mechanisms* [in Chinese], China Ocean Press, Beijing.

Zaron, E., and D. A. Jay (2014), An analysis of secular change in tides at open-ocean sites in the Pacific, *J. Phys. Oceanogr.*, *44*, 1704–1726.

Zhang, E. F., X. Q. Chen, and X. L. Wang (2003), Water discharge changes of the Changjiang River downstream Datong during dry season, *J. Geogr. Res.*, *13*(3), 355–362.

Zhang, E. F., H. H. G. Savenije, S. L. Chen, and J. Y. Chen (2012), Water abstraction along the lower Yangtze River, China, and its impact on water discharge into the estuary, *Phys. Chem. Earth*, *47–48*, 76–85.

Zhu, Q. Y., J. Guo, G. P. Liu, and J. Xu (2008), Study on representative vertical method for tidal discharge processing of Xuliujing gauging station in the Yangtze River Estuary [in Chinese], *J. China Hydrol.*, *28*(4), 61–64.